2011

Understanding the Development of Tissue Engineered Blood Vessels

Rajendra Fernando Sawh Martinez

Understanding the Development of Tissue Engineered Blood Vessels

A Thesis Submitted to the
Yale University School of Medicine
in Partial Fulfillment of the Requirements for the
Joint Degree of Doctor of Medicine and Master of Health Science

by

Mr. Rajendra Fernando Sawh Martinez

2011

ABSTRACT:

Cardiovascular disease (1) is the leading cause of death in the world. In the United States alone, the American Heart Association estimates the cost of treating CVD in 2009 to be $475.3 billion(2). Suitable autologous blood vessels are often scarce, especially for patients who require multiple procedures. There is a global demand for improved, biocompatible vascular conduits to address these shortcomings. Biodegradable tubular scaffolds are currently being evaluated as vascular grafts in the surgical treatment of cardiovascular disease. Seeding scaffolds with bone marrow-derived mononuclear cells (BMCs) prior to implantation has been shown to significantly improve outcomes. However, the role these cells play is poorly understood.

Various inferior vena cava (IVC) interposition models in recipient mouse models were used to evaluate the developmental remodeling process of engineered blood vessels. Detailed analysis of vascular graft morphology and CT imaging provide standardization of graft analysis for various TEVG models. Seeding scaffolds with BMCs significantly improved patency rates and graft development. However, seeded BMCs did not directly contribute to the cellularity of the developing vessel, and were not detectable by three weeks. Rather, BMCs were found to produce significant amounts of various cytokines in response to the scaffold biomaterials, resulting in early recruitment of recipient mouse monocytes to the scaffold and subsequent improvement in vascular neotissue formation. A series of cell-tracking experiments demonstrate vascular cell in-growth from adjacent vascular tissue. These results indicate that engineered blood vessels mature through an early cytokine induced inflammatory response that induces native tissue regeneration.

ACKNOWLEDGEMENTS:

This thesis was done under the supervision of Dr. Christopher Breuer, M.D., of the Department of Surgery, Division of Pediatric Surgery. I am eternally grateful for all his guidance, support, and mentorship during my medical school training. Additionally, I am indebted to my thesis advisors, Drs. Themis Kyriakides, Ph.D., and Jordan Pober, M.D., Ph.D., for their expert advice on this project.

I would also like to extend my warmest gratitude to the many individuals with whom I have worked and collaborated on these and other studies during my research fellowship, including Dr. Jason David Roh, M.D., Dr. Gustavo Villalona, M.D., Dr. Narutoshi Hibino, M.D., Ph.D., Dr. Edward McGuillicuddy, M.D., Dr. Tamar Mirensky, M.D., Dr. Tai Yi, M.D., Dr. Wawrzyniec Dobrucki, Ph.D., Dr. Yuji Naito, M.D., Ani Nalbandian, Dr. Lesley Devine, Ph.D., Dr. Steven Jay, Ph.D., Jaime Harrington, Dr. Nicholas Pietris M. D., Dr. Deepak Rao M.D., Daniel Duncan, Adam Shoffner, Dr. Mathew Brennan, M.D., Dr. James Dzuria, Ph.D, Dr, Albert Sinusas, M.D., Dr. Toshiharu Shinoka, M.D., Ph.D., Dr. Edward Snyder, M.D., Dr. Mark Saltzman, Ph.D., Dr. George Tellides, M.D., Ph.D. and Dr. Diane Krause M.D., Ph. D.

This project would not have been accomplished without the support and encouragement of the Office of Student Research and the Department of Surgery at Yale. Funding was obtained through the NIH T32 Predoctoral Clinical Research Fellowship, NHLBI Short-term Research Fellowship, and the Charles Ohse Grant for Surgical Research. Additional funding came from the AMA through a Foundation Seed Grant, and the NIH through KO8-HL083980, PO1-HL070295, R01-HL085416 and RO-1GM072194 grants.

Finally, I would like to thank my family and friends for all their guidance, support and love throughout the years.

Table of Contents

Table of Contents

PART I. Vascular Tissue Engineering Overview

Background:

Cardiovascular disease (CVD) is the leading cause of death in the world. Ischemic heart disease, cerebrovascular disease and peripheral vascular disease account for 13 millions deaths annually(3). Additionally congenital heart disease, which represents the most common birth defect affecting nearly 1% of all live births, remains a leading cause of death in the newborn period. In the United States alone, the American Heart Association estimates the cost of treating CVD in 2009 to be $475.3 billion(2).

For end-stage cardiovascular disease in adults, or in children with congenital cardiovascular anomalies, surgical reconstruction remains the treatment of choice. Unfortunately there is a relative paucity of autologous tissue available for reconstructive surgeries, necessitating the use of synthetic materials.

Biomaterials available in the cardiovascular surgeon's armamentarium include autologous vessels and prosthetic materials. Autologous tissue is superior to prosthetic materials such as Goretex®, as prosthetics are more prone to thrombosis, infectious complications, neointimal hyperplasia, and accelerated atherosclerosis(4-7). In an adult patient undergoing multiple cardiac or peripheral vascular procedures, however, suitable autologous tissue may be scarce due to the diffuse nature of atherosclerosis. Additionally, in children undergoing surgery for complex congenital heart defects, repairs may be extra-anatomic and require more autologous tissue than is available. Clearly, there is demand for improved, biocompatible vascular conduits in these populations.

The great promise and hope of vascular tissue engineering is the development of biological substitutes that restore, maintain or improve tissue function. The origins of

vascular tissue engineering can be traced back to Alexis Carrel who received the Nobel Prize in medicine for his early work in vascular biology. This established the basic principles that provided the foundation for vascular surgery. Later in his career while working in collaboration with Charles Lindbergh at the Rockefeller Institute, some of the early pioneering work in cell culture was performed. In their manuscript entitled "The Culture of Whole Organs," Carrel and Lindbergh postulated that cell culture would one day be used to grow entire organs(8). However it was not until Weinberg and Bell's seminal paper in 1986 that Lindberg and Carrel's prediction became a reality for vascular tissue(9). This search led to many advances in our basic understanding of tissue interactions, including the critical importance of cellular and matrix interactions, the modulation of cellular recruitment, growth and differentiation, as well as a deeper appreciation for the challenges that are faced in attempting to apply these discoveries clinically. The purpose of this introduction is to guide the reader through the major milestones of vascular tissue engineering while providing in detail rationale for the importance of continued scientific investigations, including this current study, aimed at reducing the tremendous burden of cardiovascular disease.

Historical Overview

The first report of the use of synthetic vascular grafts dates back to 1952 when Voorhees *et al.*. used Vinyon N cloth tubes as arterial interpositions in dogs(10-13). Prior to this report, scientists were focused on using native arteries as conduits(10, 13). In the ensuing years, other synthetic materials aimed at passively transporting blood with minimal reaction were developed, leading to the clinical success of polyethylene terephthalate (Dacron) and expanded poly tetrafluoroethylene (ePTFE).

Major achievements in creating an ideal conduit have driven the continued search for the best strategy to create fully functioning blood vessel substitutes. In 1986, Weinberg and Bell's landmark publication described the use of bovine cells with rat collagen gel to create an artificial blood vessel model. In 1998, Shinoka *et al.,* first described the use of a biodegradable synthetic scaffold with ovine cells, demonstrating long-term autologous implantation in a low pressure pulmonary artery system(14). Also in 1998, L'Heureux *et al.,* published their creation of an engineered graft that used human cells and was tested as a short-term xenogeneic implant in a high pressure arterial bypass model(15). In 1999, Nicklason *et al.* and Shum-Tim *et al.* described the creation of an artery grown *in-vitro* using autologous porcine/ovine cells on a biodegradable polymer(16, 17). In their studies, Niklason *et al.,* used small diameter grafts, and studied their vessels under arterial pressures in the short-term. Shum-Tim *et al.,* developed large diameter grafts, studied under lower pressures with long-term evaluation of function.

In 2001, Shin'oka *et al.*, reported the first clinical use of a tissue-engineered vascular construct. The vascular graft was implanted in a four-year old girl to reconstruct an occluded pulmonary artery, after a previous Fontan procedure(18). In another major milestone for vascular tissue engineering, in 2007 L'Heureux *et al.* used their sheet-based tissue engineered blood vessel clinically as replacements for failing arteriovenous shunts(19). Despite these tremendous achievements, the field has yet to report the clinical use of a tissue-engineered vascular construct as a fully arterial interposition in humans. Further, the mainstay therapy for vascular reconstruction continues to be autologous arteries and veins. In the following pages we will detail these early successes,

discuss the applications of vascular tissue engineering in clinical trials, and describe the frontiers of our technology.

Critical Elements of an Artificial Blood Vessel

Synthetic vascular grafts were developed for patients with insufficient autologous tissue for bypass grafting. These grafts have reasonable safety profiles, satisfactory surgical handling characteristics (i.e. suture retention), and are available "off-the-shelf" for use as large caliber bypass grafts. Currently available synthetic vascular conduits, however, have several significant limitations. These grafts have no growth potential, thus many pediatric patients will "outgrow" the graft and require re-operation. Re-do operations are associated with an increased risk of complications and death. Bioprosthetic materials such as gluteraldehyde-fixed xeno- or allografts used for grafting are prone to ectopic calcification, resulting in poor durability. Both prosthetic and bioprosthetic materials are prone to infection, putting the patient at risk for sepsis, graft rupture, distal septic emboli, as well as re-operation for explantation of graft material. Lastly, the use of synthetic grafts as small caliber bypass grafts is limited as they are prone to thrombosis and neointimal hyperplasia, likely from a lack of biocompatibility and an inability to repair and remodel.

Tissue-engineered vascular conduits address the shortcomings of currently available vascular conduits. The ideal tissue-engineered graft possesses excellent surgical handling characteristics. An experienced surgeon must be able to handle the graft, modify it as necessary for the patient's anatomy, perform anatosmoses using standard surgical technique and instrumentation, and obtain hemostasis immediately

following implantation. Because of the morbidity and mortality associated with longer operative and anesthetic time, the surgeon must perform these anastomoses in a timely fashion. Optimally, tissue-engineered grafts would be available "off-the shelf" (similar to prosthetic grafts), and require minimal manipulation other than seeding the cell on the substrate the day of surgery.

In addition to satisfactory surgical handling techniques, the ideal tissue-engineered vascular graft is biocompatible. The polymerized scaffold or decellularized matrix should degrade over time, leaving intact vascular neotissue that provides the structural integrity for the conduit. The degradation of scaffold materials results in a completely biocompatible structure that is not prone to infection or ectopic calcification, and does not require immunosuppression. Finally, the ideal tissue-engineered graft possesses the intrinsic ability to grow with the patient, obviating the need for re-operations in the pediatric population.

The most important characteristic of a tissue-engineered vascular graft is, however, recapitulation of vessel form and function. Put simply, grafts implanted in the arterial and venous circulation should mirror as closely as possible the native artery and vein. The ideal arterial interposition graft possess a functional, confluent, non-thrombogenic endothelium and a thick smooth muscle laden tunica media that can accommodate mean arterial pressure and constrict appropriately to ensure perfusion to end-organs during low flow states. Thus, the intrinsic mechanical strength of the seeded scaffold should be higher and the degradation time longer in arterial grafts than in venous grafts where mechanical integrity is less critical but adequate compliance is necessary.

Approaches to creating TEBVs

The first artificial artery: Weinberg and Bell

The first reported successful construction of a tissue-engineered vascular graft came from Weinberg and Bell in 1986. Prior work had established the use of synthetic materials as vascular conduits, albeit not for small diameter vessels (<6mm diameter), and autologous tissue had become the mainstay of vascular repair. Building on previous reports of partial vascular constructs, including *in vitro* growth of endothelial cells and models of the vascular wall in mock circulatory loops, this seminal paper reported culturing bovine vascular cells to seed a collagen matrix in an tubular mold(9, 20).

Specifically, bovine smooth muscle cells were combined with collagen using a casting culture medium to create a tubular lattice. After a week of culture, a synthetic Dacron sleeve was placed on the outer surface of the construct, and seeded with fibroblasts to create a neo-adventitia. After another two weeks, the grafts were seeded with endothelial cells and left in a rotational culture (1rev/min) for one week. This procedure provided a template for the creation of a tubular cellular structure that demonstrated extracellular matrix deposition of collagen, alignment of smooth muscle cells and a confluent endothelial cell layer, in a construct that had burst pressures of up to 323 mmHg when reinforced with added layers of Dacron. This led the authors to describe the use of their graft as a model for the study of the biological properties of blood vessels, rather than as a potentially clinically useful construct. Despite these shortcomings, Weinberg and Bell laid the foundation and provided a roadmap for scientists to develop artificial blood vessels, as their publication marked the birth of vascular tissue engineering.

First clinical use of a TEBV

Congenital cardiac anomalies, a diverse spectrum of defects, result in significant perinatal morbidity and mortality. Untreated single ventricle anomalies are associated with 70% mortality in the first year of life. The therapy of choice is surgical reconstruction. Without surgery, survival of this cohort into adulthood is rare. Initially described in 1971, the Fontan operation separates pulmonic and systemic blood flow; subsequently decreasing the incidence of chronic hypoxia and high output cardiac failure. This suite of procedures requires a synthetic graft, commonly Polytetrafluoroethylene (PTFE, or Gore-Tex®). As mentioned above, PTFE has several limitations, including potential for infection, thrombosis, and ectopic calcification(21-23). Furthermore, PTFE does not grow, resulting in patients "outgrowing" the graft and requiring re-operation, or suffering complications related to intentional graft over-sizing.

The fabrication and seeding of biodegradable polymer scaffolds for use in humans was an outgrowth of work performed in large animal models. Precursors to the clinical study included the creation of a tissue-engineered heart valve by Zund and others(24-27). This valve construct consisted of biodegradable polyglycolic acid fibers serially seeded with fibroblasts and endothelial cells. These tissue-engineered valvular constructs were implanted in the pulmonary valve position in juvenile lambs. Functional performance of the grafts was satisfactory on ultrasound, and histological analysis revealed appropriate cellular architecture. These results were validated by a larger study with acellular valve controls, in which the seeded scaffolds demonstrated superior functionality(28).

The natural extension of tissue-engineered heart valves was the creation of tissue-engineered vascular conduits. These tubular constructs could be fabricated from the

same scaffold materials and cellular elements, with the additional advantage of less complex biomechanical constraints(17, 29, 30).

Although both tissue-engineered heart valves and blood vessels demonstrated mechanical integrity and vascular neotissue formation *in vivo*, the original seeding models relied on time-consuming expansion of endothelial cells and smooth muscle cells *in vitro.* This made experiments time consuming and vulnerable to culture contamination, in addition to limiting the practicality of human use, as each patient would require multiple(31). Attention was turned to other sources of seeded cells, with a focus on cells that could be procured on the day of surgical implantation of tissue-engineered grafts. Seeking an abundant cell source that did not require *ex vivo* tissue culture expansion, Matsumura and colleagues seeded polymer scaffolds with autologous bone marrow and implanted these constructs into the inferior vena cava of dogs(32, 33). Not only did these grafts remain patent, histological analysis revealed cell populations elaborating vascular endothelial growth factor (VEGF) and expressing endothelial or smooth muscle cell markers(32).

The first reported use of a tissue-engineered graft in humans occurred in 1999, in a four-year-old girl with a single right ventricle and pulmonary atresia(18). At the age of three she had undergone pulmonary artery angioplasty and the Fontan procedure. Subsequent angiography revealed total occlusion of the right intermediate pulmonary artery. A two-centimeter segment of peripheral vein was explanted and cells expanded *ex vivo.* Cells were seeded onto a caprolactone–polylactic acid copolymer scaffold, reinforced with woven polyglycolic acid. The occluded pulmonary artery was successfully reconstructed with the tissue-engineered graft. No postoperative

complications were reported. On follow-up angiography, the transplanted vessel was patent with no signs of aneurismal dilation.

Promising large animal study data and the first successful human application of a tissue-engineered graft provided the impetus for a larger clinical study. From May 2000 to December 2004, 25 patients (mean age 5.5 years) with single ventricle physiology were implanted with tissue-engineered grafts at Tokyo Women's Medical University. Extra cardiac total cavopulmonary connection (EC TCPC) conduits (a connection between the vena cava and the pulmonary arteries) for surgical correction of single ventricle physiology represented an ideal hemodynamic starting point for tissue-engineered grafts in humans. In this system, high flow rates minimize thrombotic risks while relatively low pressure minimizes wall tension on the conduit. This pilot study evaluated two types of scaffolds, PCLA-PGA (n=11) and PCLA-PLA (n=14). Autologous bone marrow (5 milliliters/kilogram body weight), aspirated from the patient's ilium under general anesthesia, was used to seed the polymer scaffold and the construct was incubated for two hours in media prior to implantation. All 25 patients survived to hospital discharge(34). Duplex ultrasonography, computed tomography, magnetic resonance angiography, and cineangiography were utilized for graft surveillance. All grafts remained patent, and no aneurismal dilation was detected with any imaging modality(35). Of note, six patients developed silent graft stenosis, and four underwent successful balloon angioplasty. Four patients died during follow-up (mean follow-up 5.8 years). The causes of death, however, were not related to tissue-engineered graft dysfunction; all four patients had imaging demonstrating a widely patent graft prior to death. Of the 21 surviving patients, 18 were classified as New York Heart Association

(NYHA) Class I (no impairment of physical activity) and 3 were classified as NYHA Class II (mild impairment of physical activity).

Although the Tokyo Women's study remains a landmark in tissue engineering, this data represents a single institutions experience and patients were not randomized. Additionally, although autologous bone marrow cells remain an attractive cell source for tissue-engineered graft seeding, no histological specimens exist from this clinical trial (autopsies are not usually performed in Japan, and most patients are still alive). The fate of seeded bone marrow, the optimal seeded cell number, and the role of post-operative anticoagulation remains to be determined.

Sheet-based tissue engineering

In the continuing search for an ideal conduit to repair damaged human vessels, L'Heureux et al. employed a new methodology to produce human vessels in vitro. Sheet-based tissue engineering (SBTE) employs confluent sheets of cells, and the abundant ECM they synthesize, that are grown into tubular structures to create a vessel-like structures. In developing SBTE, L'Heureux et al. sought to overcome the need to use synthetic material for structural support of biological grafts as was the case for Weinberg and Bell [9, 15, 36]. In this approach only cellular components were employed in the creation of their artificial blood vessel.

The first TEVG produced by SBTE contained only human skin fibroblasts cultured from dermal specimens removed during reductive breast surgery; smooth muscle cells and endothelial cells were isolated from newborn umbilical veins or adult saphaneous veins. Nonetheless, it had a burst pressure of 2594 ±501 mmHg [15, 37]. Cell sheets were

produced in culture medium supplemented with 50 ug/ml of sodium ascorbate, peeled off from culture flasks and tubularized around inert tubular support cylinders. After a maturation period of at least 8 weeks, the sheets become cohesive tubes that can be seeded with endothelial cells. The endothelial layer of the constructs expressed von Willenbrand factor immunohistochemical staining and demonstrated ac-LDL uptake; smooth muscle cells stained positively for alpha-smooth muscle actin and desmin. Fibroblasts did not stain for smooth muscle cell markers, but expressed vimentin and synthesized elastin, which organized in circular arrays. The ECM contained laminin, fibronectin, chondroitin sulfates and various collagen subtypes. Further research demonstrated that these artificial blood vessels retained concentration dependent contractile properties, responsive to various vasoconstricting (histamine, bradykinin, ATP) and vasodilating (sodium nitroprusside, SIN-1, forskolin) agents with and without inhibitory agents(37).

In the following years, the model was simplified to exclude smooth muscle cells and was shown to be feasible using skin fibroblasts and venous endothelium isolated from elderly patients with cardiovascular disease. Pre-clinical studies in immunodeficient nude rats, evaluated for up to 225 days, demonstrated patency rates of 85% without aneurism as abdominal aorta interpositional grafts. To study the *in vivo* development of these grafts in a more representative biomechanical environment, the tissue-engineered blood vessels were implanted in immunosuppressed cynomolgus primates. Explants at 6wks and 8wks demonstrated patent vessels with no signs of luminal narrowing or aneurismal formation. Alpha-actin positive smooth muscle cells and proteoglycan expression was also observed in both models(37, 38).

In 2007, L'Heureux and McAllister reported the second clinical use of vascular tissue-engineered constructs when they described the implantation of their tissue-engineered vascular graft in 3 patients undergoing hemodialysis treatment(19). These dialysis patients had a history of previously failed access grafts. After 24 patient-months of follow up for this cohort, only one of the grafts used for dialysis access had a thrombogenic failure, secondary to low postoperative flow rate and moderate dilatation of the graft. McAllister *et al.* then expanded their cohort to 10 patients in total, drawing from two centers, in Argentina and in Poland(39). Three out of the ten implanted grafts failed within the safety phase of their study, and one patient required surgical re-intervention to maintain patency at 11 months. These results are consistent with the expected failure rates with native hemodialysis access grafts (fistula) in such high-risk patient populations. Overall, after six months, the artificial grafts implanted as hemodialysis access grafts had a 60% primary patency rate which is superior to that of the standard of care synthetic graft (ePTFE).

Stem Cells for Vascular Tissue Engineering

During the past decade, significant attention has been turned to the use of stem cells in tissue engineered vascular grafts. Stem cells and endothelial progenitor cells can differentiate into vascular lineages and thus have the potential to repair vascular systems. Despite their obvious potential in clinical practice, there still remain many controversies regarding how EPCs actually enhance endothelial repair and neovascularization(40). Additionally, because of the limited expansion ability of EPCs, expansion of sufficient EPC populations for therapeutic angiogenesis remains a significant impediment for most

investigators. On the other hand, embryonic stem cells have an extensive self-renewal activity and can be expanded without limit, thus ES-cell-derived endothelial cells may be feasible as a novel cell source for therapeutic angiogenesis(41, 42).

Nourse and colleagues used VEGF to induce differentiation of functional endothelium from human embryonic stem cells(43). Continuous VEGF treatment of embryonic stem cells resulted in a 4- to 5-fold enrichment of CD31(+) cells but did not increase endothelial proliferation rates, suggesting a primary effect on differentiation. CD31(+) cells purified from differentiating embyroid bodies up-regulated ICAM-1 and VCAM-1 in response to TNF-α, confirming their ability to function as endothelial cells. Collagen gel constructs containing the human embryonic stem cell derived endothelial cells and implanted into infarcted nude rat hearts formed dense networks of patent vessels filled with host blood cells. Thus Nourse et al. demonstrated the ability of human embryonic stem cell derived endothelial cells to facilitate neovascularization of tissue-engineered constructs.

In addition to driving ES cells into an endothelial lineage, investigators have turned to embryonic stem cell derived smooth muscle cells as a potential cell source in cardiovascular tissue engineering(44, 45). NADPH oxidase (Nox4) over-expression in embryonic stem cell culture resulted in increased smooth muscle cell marker production, whereas knockdown of Nox4 induced a decrease in production. Moreover, Nox4 was demonstrated to drive smooth muscle differentiation through generation of H_2O_2(46). Thus Nox4 expression maintains differentiation status and functional features of stem cell-derived smooth muscle cells, highlighting its impact on vessel formation *in vivo*. It is clear that embryonic stem cells and endothelial progenitor cells will be important in

vascular tissue engineering in the future, and endothelial cell and smooth muscle cells derived from embryonic stem cell culture will require further characterization.

Autologous, readily available, bone marrow mononuclear cells (BMC) in both human and animal models promote angiogenesis, early endothelialization, and contain multi-potent cells that can also form part of the growing neovessel (47). In trying to develop a TEVG, Matsumana et al, reported initial success with the use of harvested vessel wall cells after isolation and culture. They found that this was a time consuming process that required previous hospitalization for vessel harvesting and that in half of the cases they were not able to obtain sufficient cells on the day of surgery. As a result, this group turned to BMC as the cell source for their constructs, removing the impediments of long-term cell culture and contamination, and more importantly, providing sufficient cells for the seeding of biodegradable scaffolds (35, 48-50). In the first human clinical trial with long term follow up (51), twenty-five TEVG were implanted using autologous BM derived mononuclear cells with no evidence of aneurysm formation, graft rupture, graft infection, or ectopic calcification; four patients had graft stenosis and underwent successful percutaneous angioplasty. These initial findings demonstrated the feasibility and safety of this technique and provided evidence for the use of BMC for the construction of tissue engineered vascular graft. *(Clinical studies described in detail in section 3.2)*

Summary and future directions

The history of reconstructive medicine and surgery dates back centuries as physicians and scientists have continually sought to restore function to damaged tissue.

Vascular tissue engineering began its path towards clinical utility with the construction of the first blood vessel model by Weinberg and Bell. In the ensuing years, several major breakthroughs in biological vascular graft production have led this young field into its first successful clinical applications. Vigorous research continues, as these clinical trials are in their early phase; it is a matter of time before they are attempted in the United States under FDA guidance.

In the last 30 years we have witnessed the success, and the various pros and cons of the methodologies used to create neovessels. The first generation of tissue-engineered arterial grafts represent a significant step forward, but several challenges remain to be addressed. Approaches that rely on bioreactors require significant culture time, preclude "off the shelf" availability and place the conduit at risk for contamination. Also, the cell source remains challenging, as adult human SMC's have limited number of passages in vitro, precluding the development of a well-developed tunica media. Finally, standardized imaging algorithms for implanted grafts will provide a more structured analysis of graft patency, dilation, and/or stenosis.

Undoubtedly, new approaches and techniques have yet to be developed. Modern technology in polymer fabrication or assembly may yield a more ideal scaffolding material. Advances in cell culture techniques may allow for faster production of artificial tissue. Ultimately, a deeper understanding of the signaling cascades involved in cellular interactions in neotissue development will be critical to the construction of third generation grafts. Modification of the genetic and molecular constitution of cells may lead to the development of tissue with selective maturation properties. Employing particle release technology, grafts may be constructed that would elute growth factors,

cytokines or other molecular signals that may recruit host cell development onto scaffolding material, doing away with the need for cell seeding altogether.

As this technology develops, successful clinical applicability will be paramount to future implementation. The focus in the field remains on responsible development of modern tools to combat disease that affect a large portion of the population. Potential widespread use for TEBVs will be dependent on patient safety, and functionality of TEBVs that is as least equal to currently used synthetic grafts. Through landmark accomplishments and continued clinical achievements, we near the promise of artificially constructing neotissues that replicate the function of the human body.

STATEMENT OF PURPOSE:

This project was designed to elucidate the cellular and molecular mechanisms through which bone marrow-derived mononuclear cells (BMC) seeded onto a biodegradable tubular scaffold develops vascular neotissue. Specific emphasis was placed on the role and origin of seeded and native host cells in the developmental remodeling of these scaffolds into fully integrated autologous blood vessels.

HYPOTHESIS:

1. Role of Seeded Cells

Seeded bone marrow-derived mononuclear cells (BMC) contain vascular progenitor cells, which differentiate and proliferate into the mature endothelial and smooth muscle cells of the developing engineered blood vessel.

2. Tissue Regeneration

Final graft neotissue is a chimeric tissue composed of vascular cells, originating from both the bone marrow and in-growth of adjacent vascular tissue.

SPECIFIC AIMS:

1) Develop a methodology to critically evaluate neotissue formation on the entire length of small-diameter biodegradable scaffolds among differing mouse strains.

2) Evaluate the impact of cell seeding on the development of implanted tissue engineered vascular grafts.

3) Employ genetically modified mouse models to determine the impact of inflammation and platelet deficiency on patency rates and neotissue formation.

4) Distinguish the cellular origins of neotissue aggregation (bone marrow derived progenitors vs. adjacent vasculature) on tissue engineered vascular grafts.

PART II. METHODS:

I contributed to the planning, design, gathering, analysis and interpretation of all data presented. Specifically, I led the studies that 1) finalized our understanding of the role of cell seeding and cytokine signalling, 2) developed a technique to study in-vivo vascular neotissue and 3) studied the role of murine model genetic background on neotissue development. The cell tracking work was carried out in a collaboration led by Dr. Hibino and Dr. Villalona. All the work contained in this thesis is the direct result of close collaborations, contributions and expertise from all those acknowledged. Methods carried out principally by collaborators are noted.

This study was conducted in accordance with the institutional guidelines for the use and care of animals, and the institutional review board approved the experimental procedures described below. Histologic processing/embedding of samples was done by the Yale Core Center for Musculoskeletal Disorders (NIH/NIAMS AR46032). Schematic illustration in Figure 5 done by Wendy Hill.

Construction of small-diameter biodegradable scaffolds

PGA-P(CL/LA) scaffold construction:

A dual cylinder chamber molding system was constructed by Tony DeSimone (Yale University School of Medicine Machine Shop) from a 6.5mm diameter polypropylene rod. A 1.4mm diameter inner cylinder was cored through the center of the rod for a length of 30mm and gradually tapered out to 6.0mm at the inlet (below). Polyglycolic acid (PGA) nonwoven felt [ConcordiaFibers, Coventry, RI] was used for the framework of the scaffold. The PGA felt was 300μm thick with approximately 90% total

porosity. The gradual taper of the inner cylinder enabled flat PGA felt sections (6.0mm x 4.0mm) to be easily shaped into tubes during their insertion through the inlet of the dual cylinder chamber system. A 21-gauge stainless steel needle was then introduced into the opposing end to maintain the inner lumen and further compress the felt. A 50:50 copolymer sealant solution of ε-caprolactone and L-lactide (P(CL/LA)) [263,800Da, Absorbable Polymers International, Birmingham, AL] was created by dissolving the copolymer at 5% (w/v) in 1,4-dioxane. The P(CL/LA) sealant was injected into the inlet

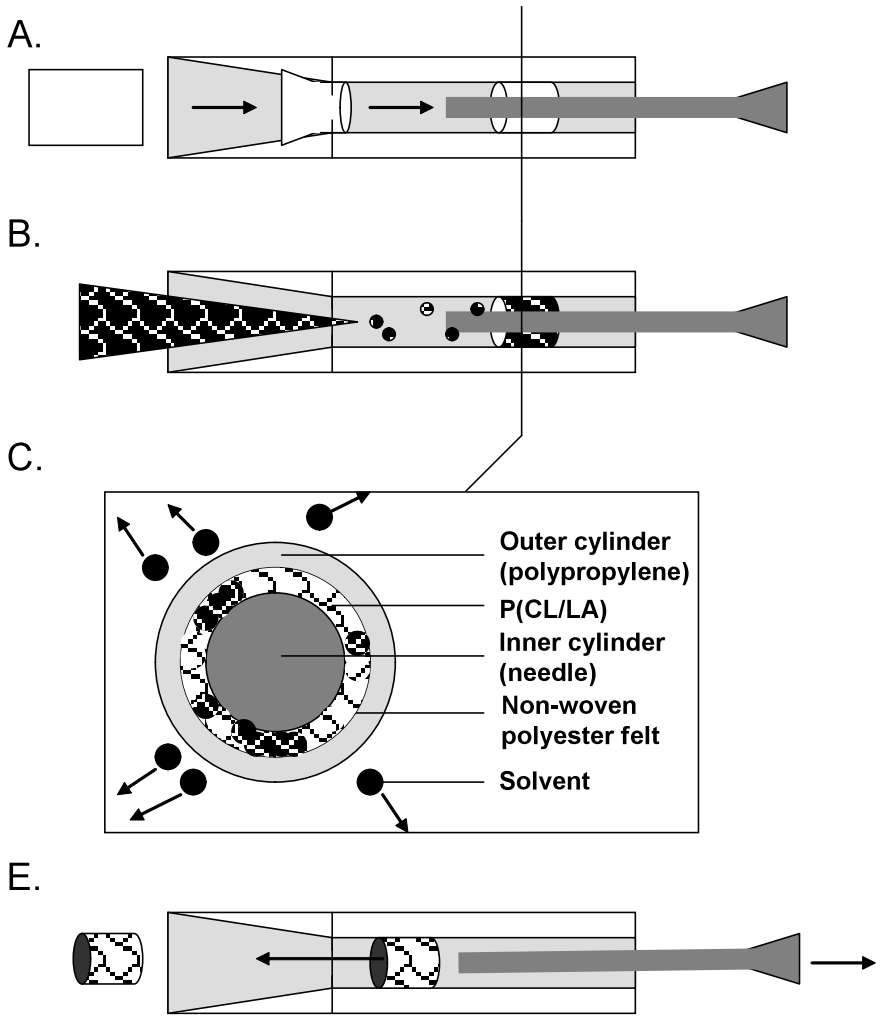

Schematic of scaffold fabrication using the dual cylinder chamber system. A) Flat PGA felts were easily rolled into tubular constructs using a gradually tapered cylinder. B) P(CL/LA) solution sealed the nonwoven PGA tube by creating an interconnecting porous structure between the PGA fibers. C) Cross sectional image demonstrating the configuration of the components and removal of solvents by lyophilization. D) Resultant hybrid polyester scaffold pushed out through inlet after

of the chamber system and allowed to penetrate the felt and fuse the open seam. The hybrid polyester scaffolds were snap-frozen at -20°C for 30 min to enable rapid transformation of the P(CL/LA) sealant from liquid to solid phase, creating a sealed tube with a newly defined porous structure of P(CL/LA) copolymer interconnecting the PGA fibers. The scaffolds were lyophilized for 24 hrs to eliminate the solvents before removing them from the dual cylinder chamber system.

Structural characterization of PGA-P(CL/LA) scaffold:

Scaffolds were cut into 0.5mm thick cross-sections and imaged on a FEI XL-30 scanning electron microscope (SEM) [Hillsboro, OR]. Lumen diameters and wall thickness were measured from high magnification SEM images.

The porosimetry profile of the scaffold was done by Tyrone Hazlett (Concordia Fibers) and acquired by micro-computed tomography (microCT) imaging [Scanco Medical microCT 40, Southeastern, PA]. Briefly, a 2048 x 2048 image matrix size over a 12.288mm field of view with 6μm slice increments was used to create an isotropic voxel size of 6μm. A total of 200-250 slices were acquired for each scaffold section, and images were then binarized by applying a small gauss noise reduction filter using fixed threshold. Three-dimensional morphometric parameters as well as thickness and separation distribution maps were generated using previously published methods(52).

Previous biomechanical characterization and biocompatibility assessment of PGA-P(CL/LA) scaffold was conducted by Dr. Jason Roh, MD.

Bone marrow-derived mononuclear cell (BMC) isolation and characterization

BMC isolation:

Murine bone marrow was isolated directly from freshly harvested mouse femur bones. A 25-gauge needle was inserted into the inter-trochanteric space and the bone marrow was flushed out with Iscove's Modified Dulbecco's Medium (IMDM). Unfractionated human bone marrow (10 donors, aged 21-44) was purchased from Lonza [Walkersville, MD].

Both human and mouse BMCs were isolated by density gradient centrifugation. Bone marrow was diluted 1:1 in sterile PBS and filtered through a 100μm nylon filter to remove bone and fat fractions. The diluted bone marrow was then layered onto either histopaque-1077 [human, Sigma] or histopaque-1083 [mouse, Sigma], and spun at 400g for 30 min. The buffy coat, containing the mononuclear cells, was collected and washed three times in sterile PBS prior to evaluating cell counts with a hemocytometer and cell viability with trypan blue exclusion.

BMC seeding onto PGA-P(CL/LA) scaffolds:

A fibrin gel solution was used to attach BMCs to the scaffold. Briefly, BMCs were suspended in a sterile fibrinogen solution (100mg/ml human fibrinogen [Sigma] in PBS) at a concentration of $2x10^6$ cells/ml. Fifty microliters of BMC-fibrinogen solution ($1x10^6$ BMCs) was statically seeded onto each scaffold. The cell solution was solidified onto the scaffold by adding 2 drops of sterile thrombin solution (100U/ml human

thrombin [Sigma] in 40mM $CaCl_2$ in PBS). Seeded scaffolds were incubated at 37°C in RPMI-1640 medium with 10% fetal bovine serum (FBS) and 1% penicillin/streptomycin (P/S) until ready to be surgically implanted. All scaffolds were implanted within 48hrs of seeding.

Characterization of human BMC sub-populations:

Isolated BMCs were characterized by fluorescence activated cell sorting (FACS). Cells were resuspended in PBS with 0.5% FBS, 0.5% human AB serum and 0.1% sodium azide, and then transferred to tubes (10^6 cells/tube) containing saturating concentrations of a cocktail of antibodies. Antibodies used were purchased from BD Biosciences [San Jose, CA] CD8 PerCP (SK1), CD14 FITC (M5E2), CD31 FITC (WM59), CD34 PE and PerCP-Cy5.5 (8G12), CD45 APC-Cy7 (2D1), CD56 PE (NCAM16.2), CD146 (P1H12), CD73 PE (AD2), CD90 FITC (5E10), 7AAD; E-Bioscience [San Diego, CA] CD3 APC (HIT3a), CD4 FITC (L3T4), CD19 (PE-Cy7); Miltenyi Biotec [Auburn, CA] CD133 APC (AC133); R&D Systems [Minneapolis, MN] VEGFR2 PE (89106); and AbD Serotec [Raleigh, NC] CD105 Alexa 647 (SN6).

To identify mature endothelial cells (EC), BMCs were incubated with CD45 APC-Cy7, CD31 FITC, CD146 PE, CD133 APC and the vital dye 7AAD (to exclude dead cells). Mature ECs were identified as being $CD45^-CD133^-CD31^+CD146^+$. Early outgrowth endothelial progenitor cells (E-EPC) were identified by staining with CD14 FITC (+ve), VEGF-R2 PE (+ve), and 7AAD (-ve). Late outgrowth EPCs (L-EPC) were identified by staining with CD45 APC-Cy7 (-ve), VEGF-R2 PE (+ve), CD133 APC (+ve), and 7AAD (-ve). Mesenchymal stem cells were identified using the panel of

antibodies recommended by Dominici et al (44). MSC were defined as $CD45^{-}CD34^{-}$ $CD105^{+}CD73^{+}CD90^{+}$ using the staining panel CD45 APC-Cy7, CD34 PE-Cy5.5, CD90 FITC, CD105 Alexa 647 and CD73 PE. Hematopoietic stem cells (53) were identified using the antibodies CD45 APC-Cy7 (+ve), CD133 APC (+ve), CD34 PE (+ve) and 7AAD. Percentages of mature lymphocyte populations were determined using the following antibodies: CD45 APC-Cy7 (+ve) for all lymphocytes; CD3 APC (+ve) and CD4 FITC (+ve) for CD4+ T cells; CD3 APC (+ve) and CD8 PerCP (+ve) for CD8 T cells; CD56 PE (+ve) and CD3 (-ve) for NK cells; and CD19 PE-Cy7 (+ve) for B-cells.

Cells were acquired on a FACSAria cell sorter and results analyzed using DIVA software [BD Bioscience] by Dr. Lesley Devine.

Cytokine release profile of human BMCs:

Human BMCs were cultured in RPMI-1640 medium supplemented with 10% FBS and 1% P/S at a concentration of $2x10^{6}$ cells/ml. Cells were stimulated with PGA-P(CL/LA) scaffolds or 10ng/ml of recombinant human interleukin-1beta [IL-1ß; R&D Systems] for 48hrs. IL-1ß, vascular endothelial growth factor (VEGF), monocyte chemoattractant protein-1 (MCP-1), and stromal derived factor-1alpha (SDF-1α) levels in the cell culture supernatant were measured using enzyme linked immunosorbent assays (ELISA) according to the manufacturer's instructions [R&D Systems].

Multiplex Luminex (Millipore) immunoassay was employed to quantify multiple cytokines simultaneously. The Luminex Assay uses dual laser capture to quantify multiple cytokines that bind to antibody-coated microbeads simultaneously and specifically. Polystyrene microspheres (5.6 microns) that carry a unique spectral signature and a cytokine specific antibody

are admixed with supernatant. Cytokines were quantified via laser capture using a Luminex 200 v .2.3 reader. 17 distinct cytokines were evaluated simultaneously – Eotaxin, Fractalkine, GCSF, GM-CSF, GRO, IFN-gamma, IL-1beta, IL-6, IP-10, MCP-1, MIP-1alpha, MIP-1beta, PDGF-BB, RANTES, sCD40L, TNF-alpha, and VEGF.

*Detection of human RNA in TEVG***.**

TEVG harvested 1, 3, 7, or 21 days post-implantation or immediately prior to implantation were snap-frozen in liquid nitrogen, and RNA was extracted by mechanical crushing over dry ice followed by incubation in RLT lysis buffer (Qiagen). Samples were passed through Qiashredder columns and processed using RNeasy mini kits according to the manufacturer's protocol (Qiagen). Reverse transcription with random hexamer and oligo-dT primers was performed according to the Multiscribe RT system protocol (Applied Biosystems). PCR reactions were prepared with TaqMan 2x PCR Master Mix and pre-developed assay reagents from Applied Biosystems (human GAPDH, Hs99999905 ml mouse HPRT, Mm00446968 ml). Species-specificity of the human and mouse probes was confirmed on human and mouse control artery segments. To determine the limits of human RNA detection, standard curves were generated by measuring human GAPDH levels obtained from 10-fold serial dilutions of hBMC in culture and hBMC seeded onto scaffolds. The limit of detection of this assay was between 10-100 cells. *PCR Analysis was conducted by Dr. Deepak Rao.*

Inferior vena cava interposition surgery

Female C.B-17 severe combined immunodeficient/beige (SCID/bg) mice, aged 3-4 months, [Taconic, Rensselaer, NY] were anesthetized with an intraperitoneal injection of xylazine and ketamine. Animals were then positioned supinely and opened with a midline abdominal incision. Using a 5X dissecting microscope [Zeiss, Thornwood, NY], infrarenal IVC was exposed, cross-clamped, and excised. Scaffolds were inserted as IVC interposition grafts using a running 10-0 nylon suture for the end-to-end proximal and distal anastomoses. All animal surgeries were done by Dr. Tai Yi. The animals were recovered from surgery and maintained without the use of any anticoagulation or antiplatelet therapy. Animals were sacrificed and grafts were explanted at various time points.

Micro computed tomography angiography

Vascular grafts were examined by microCT analysis prior to explant to evaluate patency and morphology. Animals were anesthetized with an intraperitoneal injection of xylazine and ketamine, and anticoagulated with 100IU heparin prior to sacrifice. A PE-10 [polyethylene] catheter was inserted into the thoracic IVC and 300µl of Omnipaque (300mg/ml) was injected into the venous circulation. Mice were imaged in an X-O* microCT [Gamma-Medica, Northridge, CA]. Three-dimensional reconstruction was done using COBRA software [Exxim Computing Corporation, Pleasanton, CA]. Images were combined using Total Commander [Ghisler & Co., Switzerland] and volume rendered with AMIDE imaging software [Loening, UCLA].

Micro-CTA with modified protocol:

In vivo patency and morphology of the TEVGs were evaluated 24 weeks after implantation using micro-CTA. Mice were positioned in supine position and placed on animal bed of micro-CT scanner (eXplore CT120, GE Healthcare, USA). All animals were imaged using standard micro-CT imaging protocol (220 views, 16 ms X-ray exposure time, penetration energy: 70kV/32mA). Omnipaque contrast (GE Healthcare, USA) was utilized as a contrast agent. Micro-CT images were reconstructed and visualized with MicroView (GE Healthcare, USA) and Amide (amide.sf.net) software packages to assess graft patency and vessel lumen size.

Explanted tissue engineered blood vessel characterization

Histology:

Explanted scaffolds were fixed in 10% NBF for 18 hrs and then paraffin-embedded. Unstained 5μm sections were stained with H&E, Gamori trichrome (collagen), and Verhoeff-van Gieson (elastin). Using previously published methods, some pre-implant scaffolds were embedded in glycolmethacrylate to maintain better histologic structure with processing(52).

Immunohistochemistry:

Immunohistochemical analysis was done on unstained 5μm sections using species-specific antibodies to distinguish between human seeded cells and murine host cells. Human-specific primary antibodies used were mouse-anti-human CD31 [1:100, Dako, Carpinteria, CA], CD68 [1:500, Dako], CD34 [1:2000, Abcam, Cambridge, MA], and CD45 [1:100, AbD Serotec]. Mouse-specific primary antibodies used were rat-anti-mouse Mac-3 [1:50, BD Bioscience], F4/80 [1:2000, AbD Serotec], IL-1ß [1:100, R&D

Systems], and goat-anti-mouse VEGF-R2 [1:50, R&D Systems, minimal cross-reactivity]. Primary antibodies that cross-reacted with both species were mouse-anti-human α-smooth muscle actin (αSMA) [1:1000, Dako], rabbit-anti-human von Willebrand Factor (vWF) [1:2000, Dako], and mouse-anti-human VEGF [1:100, Santa Cruz Biotech, CA]. Rabbit-anti-mouse to c-kit (Abcam), mouse-anti-mouse to Sox-2 (R&D Systems), and rat-anti-mouse Sca-1 (R&D Systems)Antibody binding was detected using appropriate biotinylated secondary antibodies [Vector], followed by binding of streptavidin-HRP [Vector] and color development with DAB [Vector]. Nuclei were then counterstained with hematoxylin. For vWF detection, a goat-anti-rabbit IgG-Alexa Fluor 568 [1:500, Molecular Probes, Eugene, OR] was used with subsequent 4',6-diamidino-2-phenylindole (DAPI) nuclear counterstaining [Vector].

Quantitative cellular analysis:

To evaluate the cellular development of the scaffolds, the cellularity at each time point (n=2-7) was measured by taking representative images of explanted scaffold cross-sections. Two 5μm cross-sections, located at approximately 1/3 and 2/3 the distance from the proximal to distal anastamosis, of each scaffold were stained with H&E. Six photomicrographs were taken at 400X magnification to represent the entire cross-section, and cell nuclei were counted and averaged.

Scaffolds explanted at post-operative wk 1 were also stained with an anti-F4/80 antibody, by methods described above, to specifically evaluate the early recruitment of mouse monocytes to the scaffold. Again, two cross-sections, located at 1/3 and 2/3 the distance from the proximal to distal anastamosis were examined. Six photomicrographs

were taken at 400X magnification to represent the entire cross-section, and F4/80 positive cells were counted and averaged.

Further explants were sectioned at specified intervals throughout the length of TEVG scaffolds (3mm) with systematic measurements of graft morphology, including explant diameter, radius, lumen circumference, outer graft circumference, and lumen surface area. Measurements were conducted in triplicate and compared across samples and within samples.

Development of MCP-1 eluting scaffold:

MCP-1 encapsulation in alginate microspheres:

Alginate microspheres, encapsulating recombinant human MCP-1 [R&D Systems], were prepared by Steven Jay using a modification of an emulsification technique developed by Zheng et al (46). Briefly, endotoxin-free alginate (18mg/ml) and hydroxypropylmethylcellulose (HPMC) (2mg/ml) [Sigma] were co-dissolved in ultrapure water, followed by direct dissolution of MCP-1 (50:1) at 1mg/ml. The resulting solution was added to iso-octane + 5% (v/v) Span 80 while homogenizing at 17,500rpm. Tween 80 was added to the emulsion in order to create a favorable HLB value for microsphere formation. After mixing, filtered 700mM $CaCl_2$ solution or filtered 700mM $ZnCl_2$ solution (pH=7) was added at a rate of 3ml/min to cross-link the alginate. Microspheres were cured, spun down at 4,000rpm, and washed twice in 2-propanol. Microspheres were then air-dried, resuspended in sterile water, and lyophilized. $ZnCl_2$ cross-linked microspheres underwent an additional immersion in M199 medium for 4 hrs, and were again filtered and lyophilized. All MCP-1 alginate microspheres were stored at -20^{o}C

until use. $ZnCl_2$ and $CaCl_2$ cross-linked particles were used at a ratio of 1:1 for all experiments. *This work was carried out by Dr. Jason Roh, Dr. Steven Jay and RFSM.*

Incorporation of MCP-1 microspheres in scaffold:

MCP-1 alginate microspheres (50mg/ml) were suspended in a 5% (w/v) solution of P(CL/LA) in 1,4-dioxane. Scaffolds were then constructed using the dual cylinder chamber system according to methods outlined above. Characterization of the microspheres embedded in the scaffold was done using scanning electron microscopy.

Controlled release profile of MCP-1 eluting scaffolds:

MCP-1 eluting scaffolds (n=4) were immersed in 1ml of M199 medium and incubated in a 37°C orbital shaker. At 1, 2, 4, 8, 12, 24, 48, 72, 96, 120, 144, and 168 hrs, the medium was collected and replaced with 1ml of fresh M199 medium. Media samples were stored at -20°C until analysis. MCP-1 content in the samples was quantified by ELISA according to the manufacturer's instructions [R&D Systems].

Transgenic Animals

Transgenic inbred C57BL/6 mice that express green fluorescent protein (GFP) under the control of ubiquitin-C promoter were obtained from the (Jackson Laboratory, Bar Harbor, Maine) and bred in our laboratories. Other transgenic animal models used are described above and elsewhere. All animal procedures were approved by the Institutional Animal Care & Committee (IACUC) at Yale University.

Fate of TEVG Seeded Cells

Six to eight-week-old (20-25 grams) C57BL/6 mice underwent implantation of IVC interposition grafts using a previously approved protocol, seeded with 1 x 10^6 cells of GFP (+) BMMC. Mice were sacrificed post-operatively at 6-hours (N=4), 1-day (N=4), 3-days (N=4), 7-days (N=4) and 14-days (N=4) and the grafts were explanted at discrete time points to asses for fate of seeded cells using quantitative real time PCR.

Cell Quantification Assay

The cellularity of each GFP (+) BMMC seeded scaffolds was determined by measuring the DNA content with the PicoGreen detection assay (Molecular Probes, Eugene, OR). At 6-hours, 1-day, 3-days and 7-days of incubation, seeded scaffold sections were rinsed three times in 1mL PBS, placed in 200uL of distilled water, and stored at -80C. At the time of evaluation, scaffold sections were thawed at 37.8C. A black 96-well plate was loaded with 50 uL from each sample. A 30ul aliquot of the PicoGreen dye was mixed thoroughly with 6ml of Tris-EDTA buffer (pH 7.5) and 50ul was added to each sample in the 96-well plate. All samples were performed in triplicate. The plate was incubated in the dark at room temperature for 10 minutes. Fluorescence was measured at 488 nm excitation and 525 nm emission. The number of cells maintained on each scaffold was determined from a standard curve generated from a known quantity of mouse BMMC. A negative control of unseeded scaffold sections was used for comparison (Roh et al., 2007)(Villalona et al 2010).

Cell Viability Assay

In order to determine GFP+ BM-MNC viability following seeding onto scaffold sections and incubation at 6-hours, 1-day, 3-days and 7-days a CellTiter 96® AQ_{ueous} Non-Radioactive Cell Proliferation Assay (Promega BioSciences, San Luis Obispo, CA) was performed. After seeding, all scaffold sections were incubated in 2ml of RPMI 1640 media (1% penicillin/streptomycin and 10% fetal bovine serum) for the respective incubation times. Media was changed every two days. Following incubation, the scaffold sections were washed 3 times with 1ml PBS and the assay reagent (tetrazolium compound (3-(4,5-dimethylthiazol-2-yl)-5-(3-carboxymethoxyphenyl)-2-(4-sulfophenyl)-2H-tetrazolium, inner salt; MTS) and an electron coupling reagent (phenazine methosulfate; PMS)) was added to each scaffold section in a 1:4 ratio with media and allowed to incubate for 4 hours at 37C. After 4 hours, a 100ul aliquot of each sample was added to a clear 96-well plate and the absorbance at 490nm was read. The relative cell viability was determined by the ratio of absorbance from the seeded scaffold sections incubated at different time points.

Bone Marrow Transplantation

After myeloablation with 900cGy total body irradiation using a 137 Cs source, six-week old female wild-type C57BL/6 mice received a tail vein injection of $5x10^6$ unfractionated nucleated bone marrow cells harvested from age matched, gender mismatched (male) GFP (+) transgenic mice, as previously described (Di Lorenzo et al., 2009). We confirmed engraftment of the bone marrow one month after bone marrow transplantation by determining the percentage of GFP (+) cells on peripheral blood using FACS. Subsequently TEVG (N=57) were implanted as IVC interposition grafts.

Specimens for immunostaining (N=27) were explanted on post-operative day 3 (N=6), 7 (N=6), 14 (N=5), 10 weeks (N=5) and 6 months (N=5) and specimens for qPCR (N=30) were explanted on post-operative day 3 (N=6), 7 (N=6), 14 (N=6), 10 weeks (N=6) and 6 months (N=6).

Composite graft

The vena cava was harvested from a male mouse. One-millimeter sections of the vena cava were anastomosed to the distal end of a scaffold. The composite scaffold was then seeded and incubated as described above. The composite TEVG was implanted in a female host (N=8). Specimens were harvested on post-operative day 7 (N=2), 14 (N=2), at 10 weeks (N=2) and 6 months (N=2).

Quantitative Real Time PCR (qRT-PCR)

Explanted tissue grafts were incubated overnight in 180 μl of lysis buffer (QIAGEN) and proteinase K (12 mAu/reaction) at 56°C. Following tissue digestion, DNA was isolated from samples using DNeasy Blood and Tissue Kit (QIAGEN) following manufacturer's instructions. The following primers and TaqMan probe were designed to amplify a specific 93 bp region of the GFP gene: forward, 5'-ACCACATGAAGCAGCACGACTTCT-3'; reverse, 5'-TGTAGT TGCCGTCGTCCTTGAAGA-3'; probe, 5'-AAGGCTACGTCCAGGAGCGCACC AT-3'. DNA amplification and quantification was performed using iCycler iQ Real-Time PCR Detection System (Bio-Rad, Hercules, CA, USA). Each qPCR reaction consisted of

the following steps: 2 min UNG incubation at 50°C to remove possible amplicon contamination, followed by 10 min at 95°C to activate the polymerase, and 40 cycles of 15 sec denaturing at 95°C and 1 min at 60°C of extension and annealing. Data were collected at the end of each elongation step and analyzed with iCycler iQ Real Time Detection System Software (Bio-rad).

Fluorescent in situ Hybridization (FISH)

FISH was performed on paraffin sections using digoxigenin-labeled mouse Y chromosome probe detected using a Rhodamine-conjugated antibody to digoxigenin (Roche Diagnostics, Mannheim, Germany) as previously described (Jones et al., 1996)(Krauss et al., 2001). Counting of Y-positive nuclei was accomplished by systematically examining the FISH-stained tissue, field by field, under 40X magnification, using a Zeiss Axiovert 200M Fluorescence/Live cell Imaging Microscope (Carl Zeiss Imaging Solutions, Thornwood, NY). Digital images were acquired using the Zeiss LSM510 confocal computer system (Carl Zeiss Imaging Solutions, Thornwood, NY). Images were pseudocolored using image processing software (Adobe Photoshop, San Jose, CA). Cell counts were obtained by first counting all of the Y chromosome-positive cells in a defined area on the tissue, and then counting the total number of cells in that area using the immunostained photographs.

Statistical analysis:

Statistical differences were measured using a Student's t-test. P values less than 0.05 were considered statistically significant.

Part III. Results

Human BMC-seeded biodegradable scaffolds transform into functional blood vessels in the SCID/bg mouse

The first objective of this study was to determine if the SCID/bg mouse could be utilized as an animal model to study human TEVG development. Specifically, we looked to see if similar results could be obtained in the SCID/bg mouse host as compared to human recipients; i.e., that hBMC-seeded scaffolds transformed into functional venous conduits in high flow, low pressure settings. TEVG were constructed under similar conditions to the Shin'oka clinical study(18) protocol (6-8), and followed over a 24 wk course as IVC interposition grafts. All hBMC-seeded TEVG (n=28) remained fully patent and functional as venous conduits (Fig. 1A). At 24 wks, TEVG (n=5) (Fig. 1C-D) morphologically and histologically resembled the native mouse IVC (Fig. 1F-G). As early as 10 wks, endothelial cells (EC) lined the inner lumen and were invested by a surrounding layer of SMC (Fig. 1H-I). By 24 wks, a mature vascular architecture, consisting of a confluent EC-lined intima and 1-2 layers of SMC media, were clearly defined in the neovessel (Fig. 1J). The original scaffold material had degraded by 24 wks, and was effectively replaced by a supportive adventitial layer composed of circumferentially oriented collagen fibrils (Fig. 1K-L). No elastin was detected in the TEVG or native mouse IVC.

Stem cells constitute a minor fraction of seeded hBMC

To test if seeded hBMC were differentiating into the mature vascular cells of the engineered neovessel, we first examined the phenotypes and relative abundances of cell populations within the human BMC population used for seeding (Table 1). We specifically searched for mature EC and SMC and progenitor cells capable of differentiating into mature vascular cells. Human BMC consisted mainly of mature leukocyte populations, including monocytes (10±4.7%), $CD4^+$ T cells (7.0±2.7%), $CD8^+$ T cells (7.9±2.5%), B cells (6.4±2.1%), and NK cells (3.2±1.4). A relatively high percentage of $CD146^+CD31^+CD45^-$ mature bone marrow microvascular EC (0.050±0.024%) was also present. The largest population of adult stems cells identified were $CD34^+$ hematopoietic stem cells (1.8±0.53%). $AC133^+KDR^+CD45^-$ proangiogeneic cells made up 0.0029±0.0042% of the hBMC population, while $CD90^+CD73^+CD105^+CD45^-CD34^-$ mesenchymal stem cells constituted the smallest percentage of hBMC, with yields of only 0.0013±0.00096%.

Static seeding of hBMC into scaffolds resulted in a similar distribution of cell types as in the original population, i.e., there was no obvious preference for any particular sub-population. Prior to implantation, the majority of hBMC in the scaffold were $CD45^+$ mature leukocytes (Fig. 2A). $CD31^+$ mature EC and $CD34^+$ stem cells were also identified, but in much lower numbers (Fig. 2B-C). No alpha-smooth muscle actin (αSMA) expression was detectable prior to implantation.

Seeded hBMC are not incorporated into the developing TEVG

Next, to determine if seeded hBMC were directly contributing to the vascular cell composition of the developing neovessel, we tracked the seeded hBMC using human-specific markers and immunohistochemistry. TEVG were explanted at various time points over a 24wk timecourse and stained for various hBMC surface antigens. $CD34^+$ human stem cells could no longer be detected in any of the TEVG after implantation. A small number of $CD68^+$ human monocytes and $CD31^+$ human EC could be found within the scaffold wall at 1 wk, but were not detectable after that time point (Fig. 2D-E). Lack of seeded hBMC retention was confirmed with quantitative RT-PCR, demonstrating no detectable human RNA in the scaffolds after 1 wk in the mouse host (Fig. 2I).

TEVG are composed of recruited murine host cells.

Despite the diminishing presence of seeded hBMC, overall cellularity of the TEVG increased markedly during the first week of *in vivo* development (Fig. 3A). This increased cellularity stabilized after 1 wk, and was primarily due to rapid infiltration of host mouse monocytes within the scaffold wall (Fig. 2F, 3B). Monocyte infiltration was subsequently followed by the influx of α-SMA expressing cells around the inner luminal lining (Fig. 2G). By 3 wks, partial endothelialization along the inner luminal lining could be detected (Fig. 2H), and by 24 wks, the scaffold had been replaced by a mature vascular structure (Fig. 1). Monocyte contribution to the cellularity of the TEVG diminished concomitantly with scaffold degradation.

Seeded hBMC increase early monocyte recruitment.

With direct evidence showing seeded hBMC were not present after 1 wk *in vivo*, we next investigated if they had any effect on the vascular development of TEVG by comparing the cellularity of hBMC-seeded scaffolds to unseeded scaffolds (Fig. 3A). At post-implantation days 1 and 3, no significant differences in cellularity could be detected between hBMC-seeded scaffolds and unseeded scaffolds. However, by day 7, the increase in cellularity was significantly greater for hBMC-seeded scaffolds compared to unseeded scaffolds (270±22 cells/hpf vs. 160±40 cells/hpf; $p<0.001$) (Fig. 3A). This increased cellularity was primarily due to a significantly increased infiltration of host mouse monocytes into hBMC-seeded scaffolds, as compared to unseeded scaffolds (120±20 monocytes/hpf vs. 60±12 monocytes/hpf; $p<0.001$) (Fig. 3B).

Human BMC secrete significant amounts of MCP-1 when seeded onto scaffolds.

Based on the above findings, we hypothesized that seeded hBMC were functioning via a paracrine mechanism instead of directly differentiating into the vascular cells of the developing neovessel. To investigate this potential function, we examined the interaction hBMC had with scaffold biomaterials to determine if scaffold exposure activated hBMC to secrete chemokines that could increase early monocyte recruitment. Scaffold exposure significantly increased the production of multiple cytokines and chemokines by seeded hBMC (Fig. 3C-E). In particular, significantly high levels of MCP-1 were found to be secreted by seeded hBMC (Fig. 3C, 3F). MCP-1 levels induced by hBMC seeding reached quantities comparable to MCP-1 levels used in prior arteriogenesis studies (12, 13). Based on the levels obtained, MCP-1's known function as a potent monocyte

chemokine, and its established link to postnatal neovascularization (12-15), we chose to investigate whether MCP-1 might be playing a role in TEVG development.

Local MCP-1 secretion from scaffolds increases early monocyte recruitment, mimicking seeded hBMC effects on TEVG development.

With *in vivo* data suggesting that seeded hBMC increased early monocyte recruitment and *in vitro* studies indicating hBMC secreted significant amounts of MCP-1 when seeded onto scaffold materials, we hypothesized that seeded hBMC were increasing early monocyte recruitment via MCP-1 secretion. To test this hypothesis, we developed a system that enabled us to study the effects of secreted MCP-1, independent of other cytokines potentially produced by seeded hBMC. This was accomplished by creating hBMC analogues, capable of only releasing MCP-1. To create these analogues, we encapsulated recombinant human MCP-1 into biodegradable alginate microparticles, 1-20μm in diameter, making them comparable in size to the heterogeneous population of hBMC (Fig. 4A). The microparticles were then embedded into the scaffold to mimic the MCP-1 secretion by seeded hBMC (Fig. 4B-C). Embedded microparticles released approximately 200ng of MCP-1 from the scaffold over the course of 72 hrs, which was similar to the duration of retention of seeded hBMC (Fig. 4D).

Unseeded scaffolds embedded with MCP-1 microparticles developed and functioned similarly to hBMC-seeded scaffolds when implanted as IVC interposition grafts in the SCID/bg mice. Host monocyte recruitment at 1 wk was significantly increased in MCP-1 eluting scaffolds (200±60 monocytes/hpf), compared to both hBMC-

seeded (120±20 monocytes/hpf; $p<0.05$) and unseeded (60±12 monocytes/hpf; $p<0.05$) scaffolds (Fig. 4E). Furthermore, after 10 wks *in vivo*, all MCP-1 eluting scaffolds (n=5) were functioning as patent venous conduits, and exhibited similar elements of vascular remodeling to the hBMC-seeded scaffolds. The MCP-1 eluting scaffold was fully infiltrated with host mouse monocytes, creating an external tube circumscribing an internal lumen of organized vascular neotissue, consisting of a confluent endothelial lining, smooth muscle medial layer, and circumferentially oriented collagen fibrils (Fig. 4F-K).

TEVG form neovessels that resemble native veins

Miniaturized PGA-P(CL/LA) tubular scaffolds were seeded with syngeneic BMMC and implanted into the inferior vena cava (IVC) of CB57BL/6 mice. Scaffold materials completely degraded by six months, at which point TEVGs displayed similar vascular architecture to a native vein. Three-dimensional computer tomography angiography of TEVGs at six months showed no evidence of stenosis, aneurismal dilation or thrombosis (figure 6a). Furthermore, histological characterization demonstrated a mature laminated structure, consisting of an endothelialized intimal layer and smooth muscle medial layer (figure 6b).

Fate of TEVG seeded cells

The quantity of GFP-labeled cellular DNA within scaffolds was maximal at 6-hours after over night incubation and the cellularity decreased following 1-day of incubation (figure 7a). These findings suggest the seeded cells decrease in number over time after in vitro

culture, probably not attaching to scaffold and washed off with media changes. The relative cell viability and activity of the seeded cells increased over a 7-day incubation period (figure 7b). Despite low attachment of these cells to the TEVG, these cells remain active and viable up to 7-days, suggesting that the cells are not dying with in vitro cultivation. Following this we implanted TEVG (N=30) to six to eight-week-old C57Bl/6 mice constructed by seeding the scaffold with GFP-labeled syngeneic BMMC and then harvested the scaffolds over at 6-hours, 1-day, 3-days, 7-days and 14-days quantifying the percentage of GFP DNA at various time points. We found that the seeded syngeneic cells disappeared as the scaffold became populated by host-derived cells identified as F4/80 expressing macrophages (not shown). Immunofluorescence of grafts demonstrated the presence of GFP-labeled cells within the graft at 6-hours, 1-day, 3-days, but no remaining cells at 7-days post-implantation (figure 7c). GFP DNA qPCR corroborated the findings that over the course of 14-days following implantation the concentration of GFP genomes decreased rapidly from 173 genomes/ul at 6-hours to 0.12 genomes/ul at 14-days (Figure 7d). We then standardized the GFP data to cell density to confirm that the seeded cells disappeared. The percentage of GFP (+) cells per TEVG was found to decrease from 4.37% at 6-hours to 0.02% at 14-days (Figure 7e).

Bone marrow cells are not the ultimate source of vascular neotissue

We next designed a series of experiments to determine the source of the cells that populated the scaffold. To assess the role of host bone marrow cells (BMC) in neovessels formation of our TEVG, chimeras were created by rescuing lethally irradiated C57BL/6

female mice with gender mismatch male GFP (+) total BMC from transgenic GFP-labeled mice. Donor cell engraftment in the surviving recipients was determined five weeks after bone marrow transplantation. Fluorescent activated cell sorting (FACS) analysis of peripheral blood GFP-labeled mice demonstrated 97.74% circulating GFP (+) cells in positive control mouse (figure 8a), 0.49% in negative control mouse (figure 8b) and 94.06% reconstitution in transplanted mice (figure 8c). Once chimeras were established, we implanted our TEVG into female mice. All mice were sacrificed at days 3, 7, 14-days, 10-weeks and 6-months post-implantation and all graft were harvested for histological analysis. Three and seven days after implantation, Y Chromosome (+) (Y Chr) cells were found in the graft wall, most of these male-derived BMC were macrophages determined by colocalization for FISH Y (+) cells and F4/80 antibody using immunofluorescence technique (not shown). At fourteen days as the number of BMC increased within the graft wall, the presence of endothelial cells and smooth muscle cells begin to appear. These vascular cells were positive for vWF and SMA markers, but negative for Y Chr cells (figure 8d, 8e). Ten weeks after implantation a confluent neointima (EC) and neomedia (SMC) are present; both layers are negative for YChr cells (not shown). Finally, six months post-implantation the neovessel endothelial layer is composed of vWF (+) YChr (–) cells (figure 9a). The smooth muscle layer is composed of calponin (+) YChr (–) cells (figure 9b) and the scaffold is mostly degraded with few inflammatory cells present that are positive for MAC-3 and Y Chr (+) (figure 9c). The numbers of infiltrating BM-derived YChr (+) cells in the graft wall increased up to 10 weeks, while graft degradation is occurring, but at 6 months post-implantation these cells markedly decrease (figure 9d). This acute inflammatory response and later decline was

corroborated using qPCR for GFP DNA within the graft over a six-month period (figure 9e). These experiments demonstrated that the macrophages that initially infiltrated the scaffold were of male origin. At later times a confluent layer of endothelial cells and smooth muscle cells is present in the neovessel with no evidence of co-localization of either smooth muscle cell markers or endothelial cell markers with the Y chromosome (figure 9f).

Neovessel formation arises from in-growth of vascular cells from the neighboring blood vessel

To determine if the endothelial cells or smooth muscle cells derived from the neighboring blood vessel, we developed a composite vascular graft created by anastomosing a segment of syngeneic male IVC with a TEVG (figure 10a). These composite vascular grafts (N=8) were implanted into female hosts and harvested on post-operative day 7, 14, 10-weeks and 6-months and processed for histological analysis and paraffin-embeding. All composite grafts were cut with 5um in a longitudinal fashion to include the male (donor) IVC, TEVG and female (host) IVC (figure 10a). The composite graft and neighboring IVC were then evaluated using FISH to identify the Y-chromosome. Seven and fourteen days post-implantation most of the graft wall is populated by MAC 3 (+)/Y Chr (–) cells (host origin) and no confluent endothelial or smooth muscle cells layers are noted (not shown). An endothelial (vWF +) and smooth muscle layer (calponin +) is noted initially at fourteen days and then more confluent at 10 weeks post-implantation (not shown). Finally at 6 months post-implantation, the host-derived neovessel is composed of a confluent neointima, neomedia and a neoadventitia. Detailed analysis of

the neointima and neomedia using confocal microscopy demonstrated that the percentage of Y-chromosome positive endothelial and smooth muscle cells was greatest closer to the implanted male IVC segment (figure 10b, c). These findings suggest that the resulting neovessel is not derived from seeded cells or bone marrow progenitor cells but instead through a locally mediated process of in-growth of neighboring endothelial and smooth muscle cells from the surrounding native vessel. On immunohistochemistry, 6-month sections were negative for stem cell markers and markers of progenitor cells including Sca-1, c-kit, and Sox-2.

Part IV. Discussion

In contrast to prior studies reporting that stem cells within seeded BMC differentiate into the mature vascular cells of developing TEVG (32), we found no evidence supporting this concept of a stem-cell mediated process of vascular development. While we did identify small populations of hematopoietic and vascular progenitor cells in the BMC population used for seeding (table 1), we did not detect any human-derived BMC in the mature neovessel beyond one week post-implantation (Fig. 2). Rather, our data suggests that hBMC-seeded biodegradable scaffolds transform into functional mature blood vessels via an inflammation-mediated process of vascular remodeling that is expedited by the secretion of MCP-1 from the seeded hBMC (Fig. 5A).

A paracrine role of seeded BMC in the vascular remodeling of TEVG is consistent with a number of studies reporting that transdifferentiation of bone marrow-derived stem cells *in vivo* is rare (54-59). Mechanistic studies examining the role of BMC

in cell therapies for ischemic diseases demonstrate that these cells do not differentiate into mature EC or regenerating tissue, but instead function by releasing multiple cytokines that induce therapeutic angiogenesis, arteriogenesis, and/or cytoprotection (59-63). Early reports of transdifferentiation may be attributable to misinterpretations of cell fusion (64-67). It is possible that cell fusion may also explain results of prior TEVG studies, which used fluorescent membrane labeling techniques to track seeded BMC (32). As determined in this study, monocytes/macrophages are the predominant cellular infiltrate in TEVG, and are very adept at phagocytosis and cell fusion. To avoid potential misinterpretations of cell fusion or auto fluorescence, we used peroxidase-based immunohistochemistry to track seeded hBMC in an immunodeficient mouse host. As far as we know, murine cells have never been shown to express human antigens *in vivo*. Additionally, our chimeric hBMC-SCID/bg mouse model enabled us to further validate our immunohistochemical findings with species-specific quantitative RT-PCR (Fig. 2I), a method that could not be utilized in prior studies, which employed autologous BMC sources (32, 68, 69).

What this study clearly demonstrates is that seeded BMC need not be directly incorporated into the vascular neotissue of the developing TEVG in order to produce a functional vessel. While much of the work in vascular tissue engineering has been predicated on the concept that vascular development of these biodegradable grafts is driven by seeded cells directly contributing to the mature vascular neotissue (17, 32, 33, 35, 47, 68-71), our findings suggest that seeded BMC may only play a transient indirect role in the early stages of vascular transformation. A potential limitation of our model is that the seeded BMC are human while the host is a mouse. Consequently, disappearance

of the seeded cells may be a form of xenograft rejection not relevant to the clinical setting in which autologous human cells are utilized. We think this is unlikely because the immunodeficient SCID/bg mouse strain is unable to reject human hematopoietic or vascular cells because both T cells and NK cells are defective. Despite this potential problem, we elected to study human BMC because these cells may differ in their properties from mouse BMC and effective mechanistic studies investigating their role in TEVG development cannot be done in humans.

Interestingly, our findings revealed that vascular transformation of TEVG is not driven by seeded BMC transdifferentiation and proliferation, but rather by the infiltration of host monocytes (Fig. 5A). By secreting MCP-1, seeded hBMC alter the kinetics of the early phase of vascular remodeling by expediting the recruitment of host monocytes to the scaffold (Fig. 3A-B). Rapid early monocyte recruitment has been shown to be intricately involved in postnatal blood vessel formation (72-74). In particular, successful arteriogenesis is dependent upon MCP-1 induced monocyte recruitment to pre-existent collateral arterioles (75-79). TEVG seem to follow a similar developmental pattern in which a short pulse of MCP-1 (derived from scaffold-activated BMC vs. shear stress-activated EC/SMC) enables rapid monocyte recruitment to a pre-determined location of blood vessel formation (biodegradable scaffold vs. collateral arteriole).

The exact roles recruited monocytes play in the vascular transformation of TEVG are currently under active investigation in our laboratory. We hypothesize that host monocytes have similar functions in TEVG development as they do in postnatal neovascularization, including producing an important milieu of cytokines, growth factors, and proteases necessary for vascular cell proliferation/migration and appropriate vascular

remodeling (80, 81), Fig. 5A). In particular, continued vascular endothelial growth factor (VEGF) expression has been shown to be critical in adult neovascularization for appropriate cell recruitment and prevention of neovessel regression (82-84). Our preliminary findings suggest a similar phenomenon in the vascular development of TEVG. Recruited monocytes remain within the scaffold until it fully degrades. In conjunction, we have seen VEGF expression within the scaffold wall throughout the duration of monocyte/macrophage infiltration, suggesting a continued secretion of VEGF by the infiltrating cells (Fig. 5B). Ultimately, it is likely that recruited monocytes produce not only VEGF, but multiple molecular agents, which orchestrate the proper vascular remodeling of the TEVG prior to scaffold degradation.

It must be noted that although the SCID/bg mouse has enabled us to study the same population of human BMC being used in clinical TEVG trials and provided insight into the mechanism of TEVG development, its lack of a functional adaptive immune system may have effects on this process that we are unable to detect in an immunodeficient host. Recent studies have suggested that regulatory T cells and NK cells may play a role in modulating postnatal neovascularization (85, 86). One interesting observation in the SCID/bg mouse was that a statistically significant difference in overall patency rates was not detected between BMC-seeded and unseeded scaffolds, which may be a reflection of the immunodeficient component of our mouse model. Prior studies comparing BMC-seeded versus unseeded scaffolds in various immunocompetent species have shown variable results in terms of patency, with results ranging from no significant difference to a 60% reduction in patency without BMC seeding (68, 69). Despite these discrepancies in preservation of patency, both studies reported that BMC seeding altered

vascular remodeling of the graft in terms of extracellular matrix production, organization, and cellularity. Further studies in immunocompetent mouse models will be necessary to delineate what roles the adaptive immune system and recipient host play in TEVG development. However, it is clear that BMC seeding exerts a significant effect on the vascular remodeling of TEVG. For the first time, our study shows that seeded BMC significantly affect the kinetics of vascular transformation by accelerating the rate of neovessel development through increased early monocyte recruitment.

The second series of experiments in this study sought to determine the source of the cells that make up the neotissue in our tissue engineered vascular grafts. In order to accomplish this goal, we investigated the origins of the vascular neotissue cells in a syngeneic immunocompetent mouse recipient using bone marrow chimeric hosts and composite vascular implants. Miniaturized PGA-P(CL/LA) tubular scaffolds were seeded with syngeneic BMMCs and implanted into the mouse IVC to mimic the high flow, low pressure venous setting seen in the clinical application for congenital heart surgery.

Results of this study validate our previous work demonstrating the rapid disappearance of the seeded cell from the TEVG, however this time performed in a clinically relevant, immune competent murine model (87). To trace the fate of the BMMC in this study, we implanted TEVG constructed by seeding the scaffold with GFP-labeled syngeneic bone morrow-derived mononuclear cells and then harvested the scaffolds over a 2-week time course quantifying the percentage of GFP DNA at various time points. As we had observed in the human into mouse xenogeneic model, we found that the seeded syngeneic cells disappeared as the scaffold became populated by host-

derived cells identified as F4/80 expressing macrophages. To demonstrate that this was not simply a dilutional effect due to increased cell density secondary to the infiltrating host inflammatory cells, we standardized the GFP data to cell density and confirmed that the seeded cells disappeared. Also as with previous studies in other animal models, scaffold materials completely degraded by six months, at which point TEVGs displayed similar vascular architecture to a native vein (32, 68, 69).

To analyze the role of bone marrow-derived cells in vascular neotissue formation, we implanted TEVG into female mice which had undergone bone marrow transplantation with syngeneic male bone marrow and then harvested the TEVG at various times over a six month period; we analyzed the specimens using FISH for the Y chromosome and a variety of other cellular markers including markers for macrophages (F4/80), smooth muscle cells (calponin), and endothelial cells (vWF). These experiments demonstrated that the macrophages that infiltrated the scaffold were of male origin and were therefore were derived from the bone marrow. When we looked at later times there was no evidence of co-localization of either smooth muscle cell markers or endothelial cell markers with the Y chromosome marker suggesting that the bone marrow was not the source of the definitive vascular neotissue.

To determine if the endothelial cells or smooth muscle cells derived from the neighboring blood vessel, we developed a composite vascular graft created by anastomosing a segment of syngeneic male IVC with a TEVG. These composite vascular grafts were implanted into female hosts and harvested over a six-month period. The composite graft and neighboring IVC were then evaluated using FISH to identify the Y-chromosome. Both endothelial cells and smooth muscle cells were found to contain the

Y-chromosome. In addition, the percentage of Y-chromosome positive cells was greatest closer to the implanted male IVC segment. These data suggest that definitive neovessel cells arise from in-growth of cells, mostly likely differentiated endothelial and smooth muscle cells, from the neighboring blood vessel segment. Although we cannot rule out the possibility that there is a rare population of stem cells resident within the adjacent vascular segment, we found negative immunohistochemical staining for markers of both stem cells and progenitor cells, suggesting that it is the differentiated endothelial and smooth muscle cells themselves that migrate in to create the neotissue.

In summary, this work has demonstrated the discovery of an inflammation-mediated process of vascular remodeling that underlies the mechanism by which TEVG transform into functional blood vessels *in vivo*. This mechanism of engineered vascular formation displays many parallels to natural neovascularization (i.e. collateral arteriogenesis) and may provide further insights into the biology of these processes. However, while similarities to natural processes exist, TEVG development does appear to be a distinct process of vascular formation in itself, which may have important implications for the burgeoning field of vascular tissue engineering. Our findings suggest that some of the core concepts used in engineering blood vessels from BMC-seeded biodegradable scaffolds may be fundamentally flawed. In particular, inflammatory responses to scaffold biomaterials may not necessarily be detrimental, and the importance of seeded BMC may not be their role as progenitors of cellular constituents, but rather as mediators for appropriate vascular remodeling and development.

Additionally, this study has demonstrated that the smooth muscle cells and endothelial cells that make up the intima and media of the neovessel formed in our

model, are derived from the neighboring blood vessel wall. Therefore, the cells of the neotissue are not derived from either the seeded cells or from bone marrow derived progenitors as has previously been suggested (47). While this may be a model-specific phenomenon, it suggests that neotissue formation can be a form of augmented tissue repair or regeneration. This represents a shift away from the traditional tissue engineering theory in which the seeded cells are viewed as the building blocks of the neotissue and a moves towards a new paradigm in which the tissue engineered construct promotes or augments the body's own reparative mechanisms to induce tissue regeneration.

A better understanding of how TEVG develop *in vivo* will lead to improved, second-generation TEVG. Moreover, identification of key molecules, such as MCP-1, may provide tissue engineers with the key to harnessing the body's abilities to regenerate therapeutic neovessels *in vivo* rather than having to fabricate them *in vitro*. These findings have significant implications for rationally designing improved second-generation tissue engineered grafts based on the modulation of the host response to the tissue engineered construct.

Part V. Figures

Figure 1.

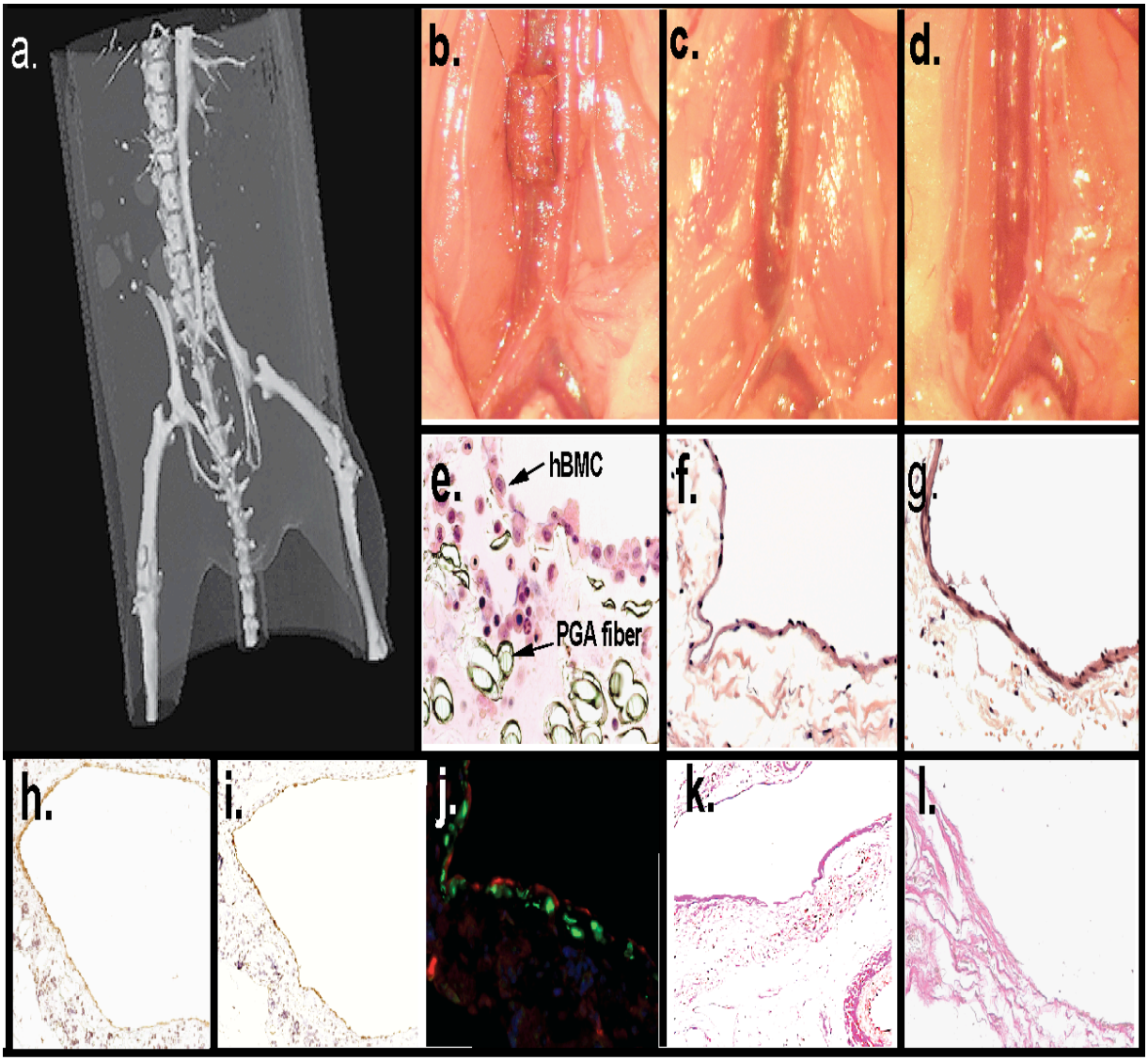

Figure 2.

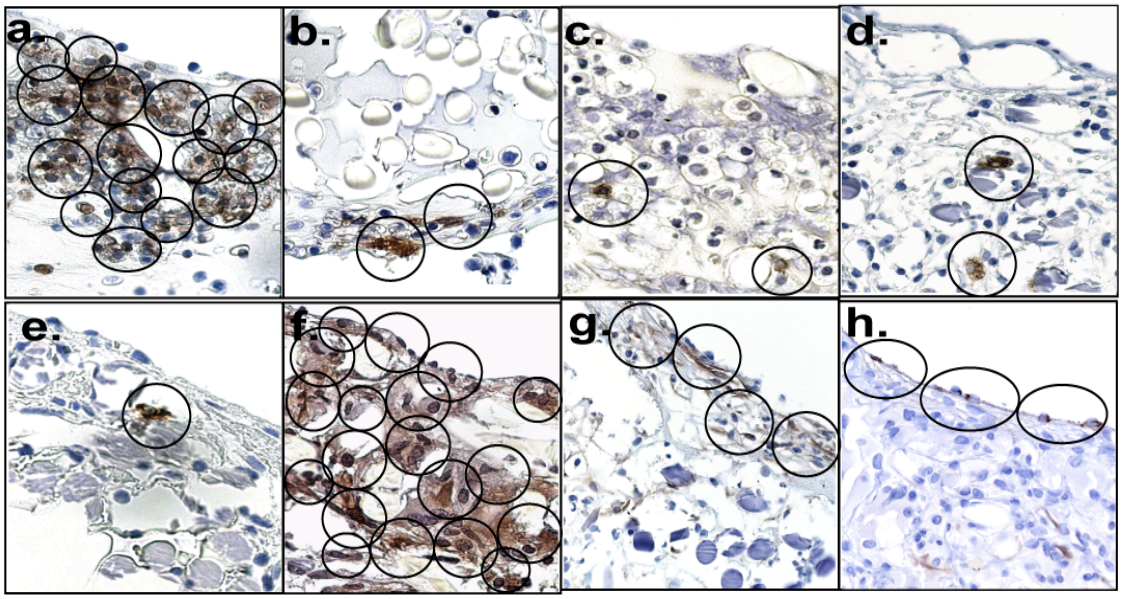
a.
b.
c.
d.
e.
f.
g.
h.

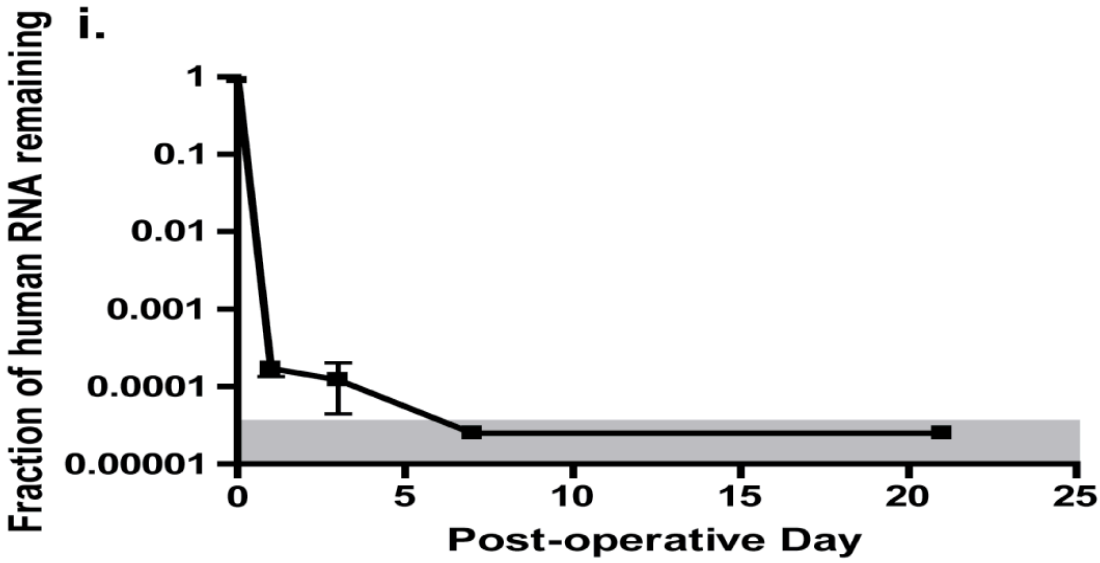
i.
Fraction of human RNA remaining
1
0.1
0.01
0.001
0.0001
0.00001
0
5
10
15
20
25
Post-operative Day

Figure 3.

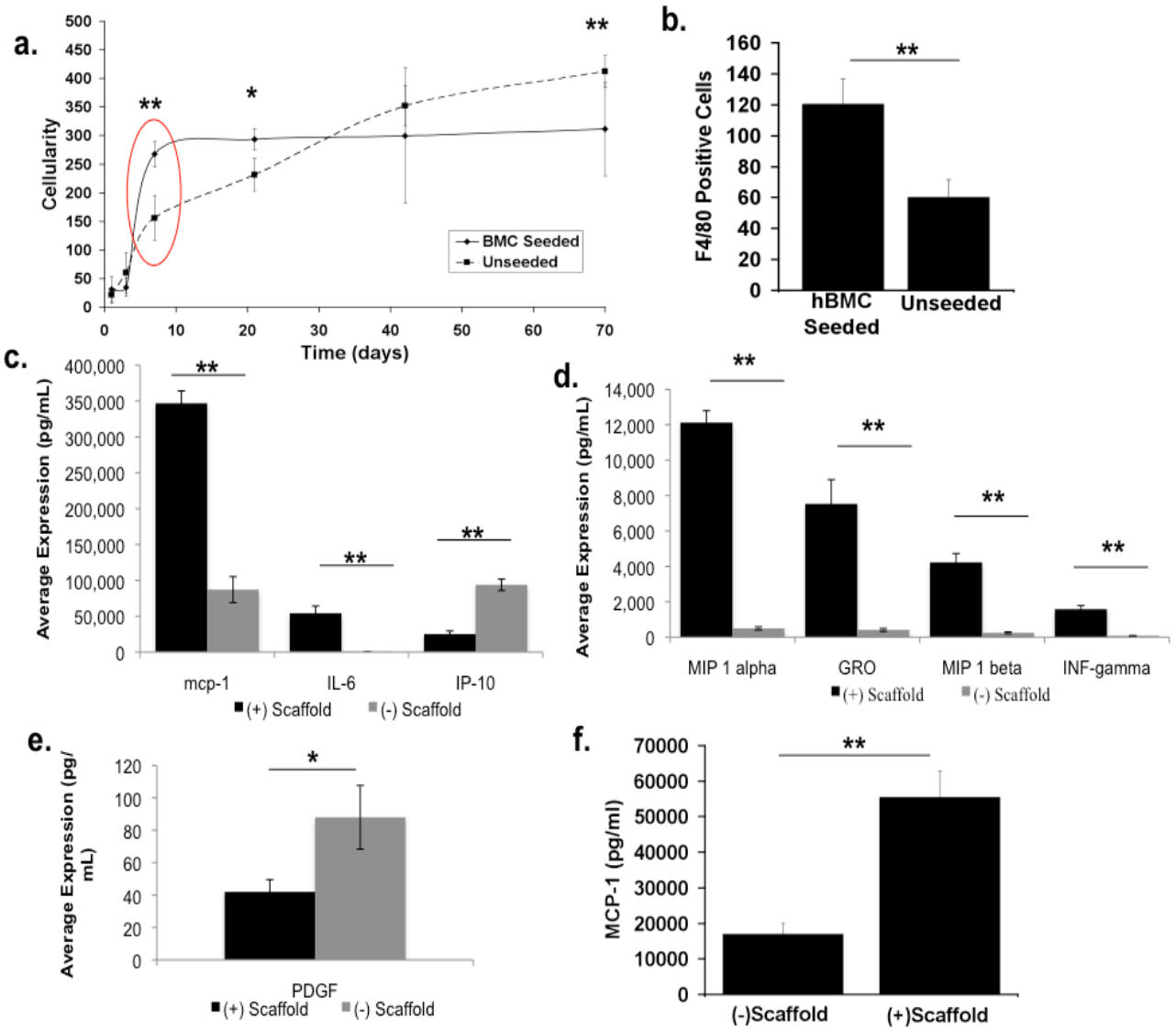
a.
Cellularity
Time (days)
BMC Seeded
Unseeded
**
*
**
b.
F4/80 Positive Cells
**
hBMC Seeded
Unseeded
c.
Average Expression (pg/mL)
**
**
**
mcp-1
IL-6
IP-10
(+) Scaffold
(-) Scaffold
d.
Average Expression (pg/mL)
**
**
**
**
MIP 1 alpha
GRO
MIP 1 beta
INF-gamma
(+) Scaffold
(-) Scaffold
e.
Average Expression (pg/mL)
*
PDGF
(+) Scaffold
(-) Scaffold
f.
MCP-1 (pg/ml)
**
(-)Scaffold
(+)Scaffold

Figure 4.

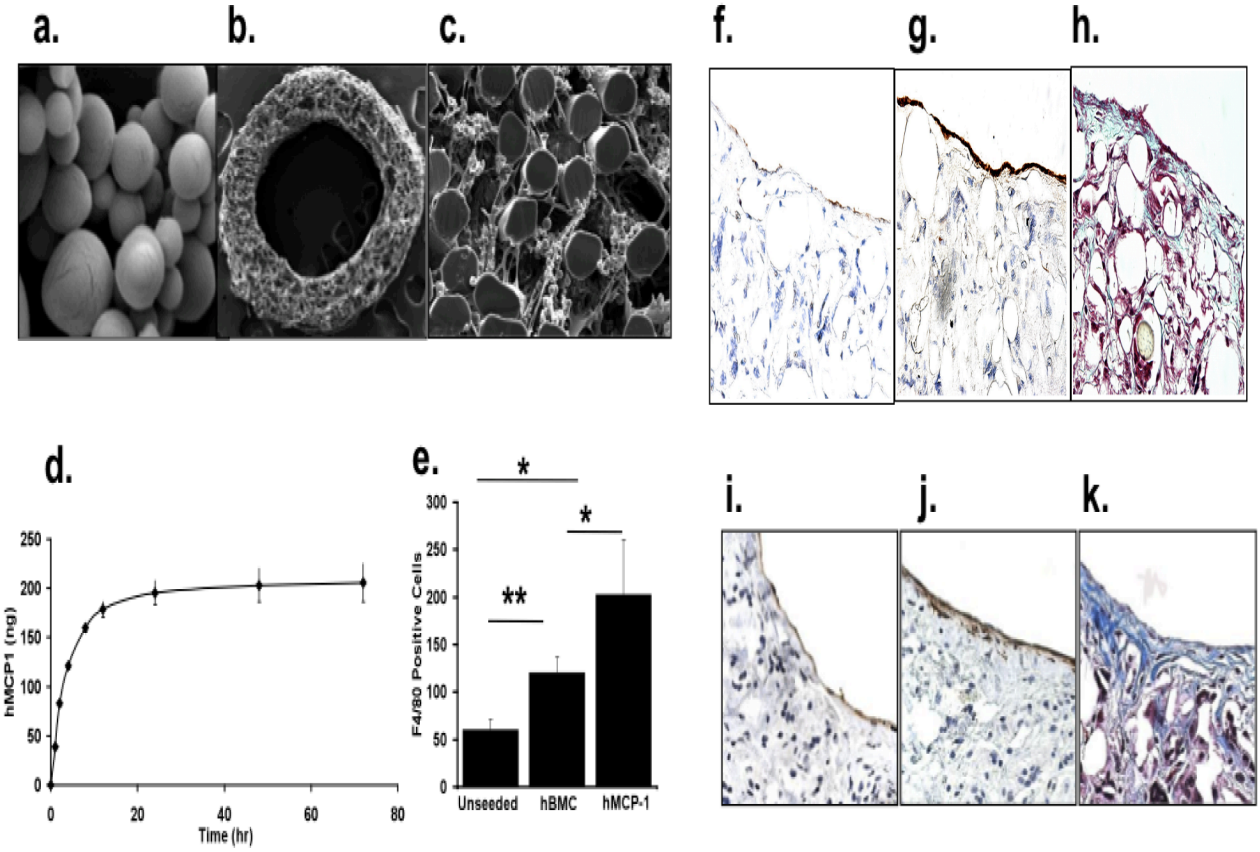
a.
b.
c.
f.
g.
h.
d.
hMCP1 (ng)
250
200
150
100
50
0
0
20
40
60
80
Time (hr)
e.
*
*
**
300
250
200
150
100
50
0
F4/80 Positive Cells
Unseeded
hBMC
hMCP-1
i.
j.
k.

Figure 5.

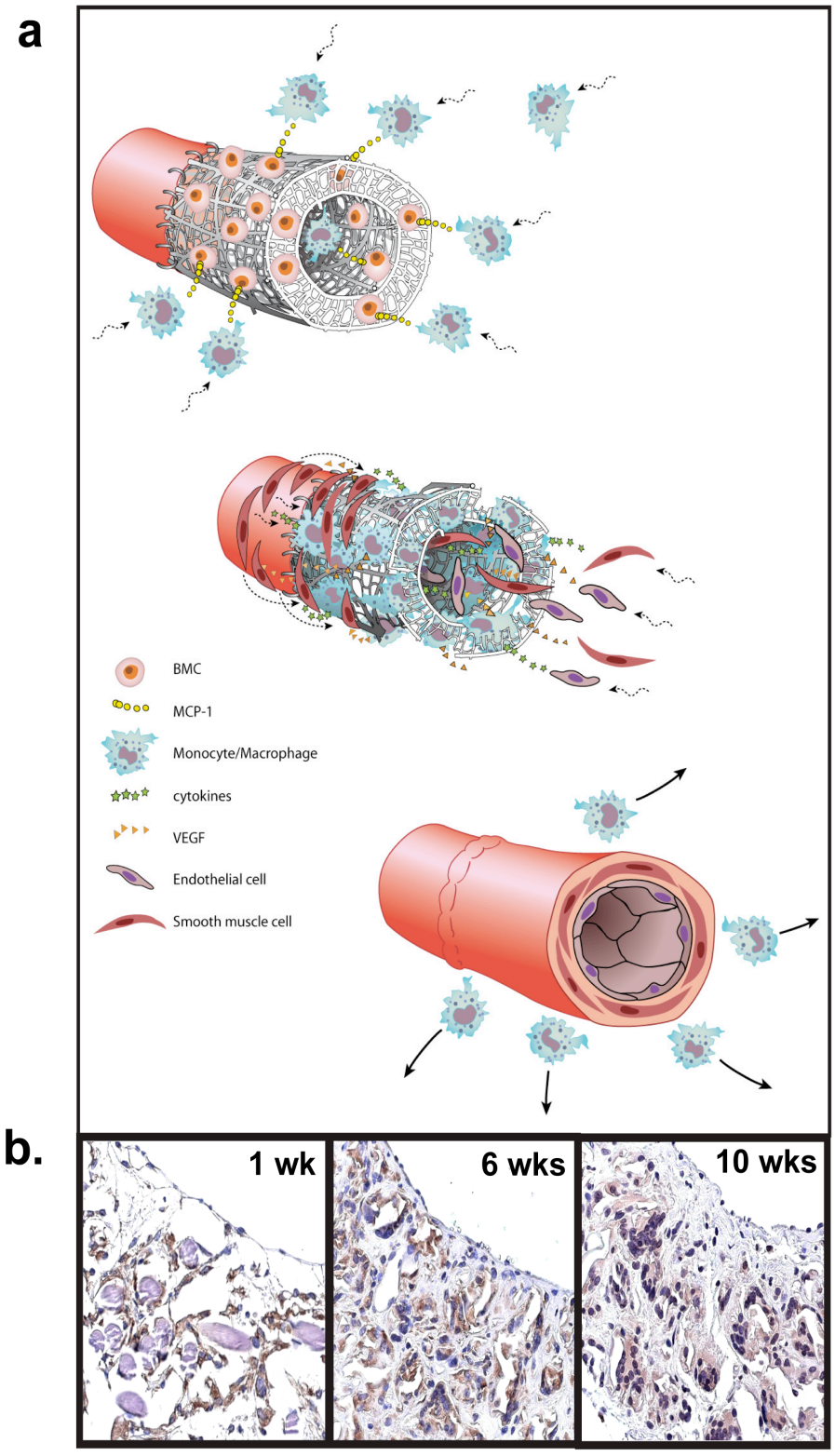
a
BMC
MCP-1
Monocyte/Macrophage
cytokines
VEGF
Endothelial cell
Smooth muscle cell
b.
1 wk
6 wks
10 wks

Table 1.

Human BMC FACS Characterization

Cell Type	Staining Panel	% BMC
Late-Outgrowth EPC	(+) AC133, VEGF-R2 (-) CD45	0.0029 ± 0.0042
Early-Outgrowth EPC	(+) CD14, VEGF-R2	1.7 ± 1.2
Mature Endothelial Cell	(+) CD31, CD146 (-) CD45	0.050 ± 0.024
Mesenchymal Stem Cell	(+) CD90, CD73, CD105 (-) CD45, CD34	0.0013 ± 0.00096
Hematopoietic Stem Cell	(+) CD34	1.8 ± 0.53
Monocyte	(+) CD45, CD14	10 ± 4.7
CD4 T Cell	(+) CD3, CD4	7.0 ± 2.7
CD8 T Cell	(+) CD3, CD8	7.9 ± 2.5
B Cell	(+) CD19	6.4 ± 2.1
Natural Killer Cell	(+) CD56	3.2 ± 1.4
Other		56 ± 10

Figure 6.

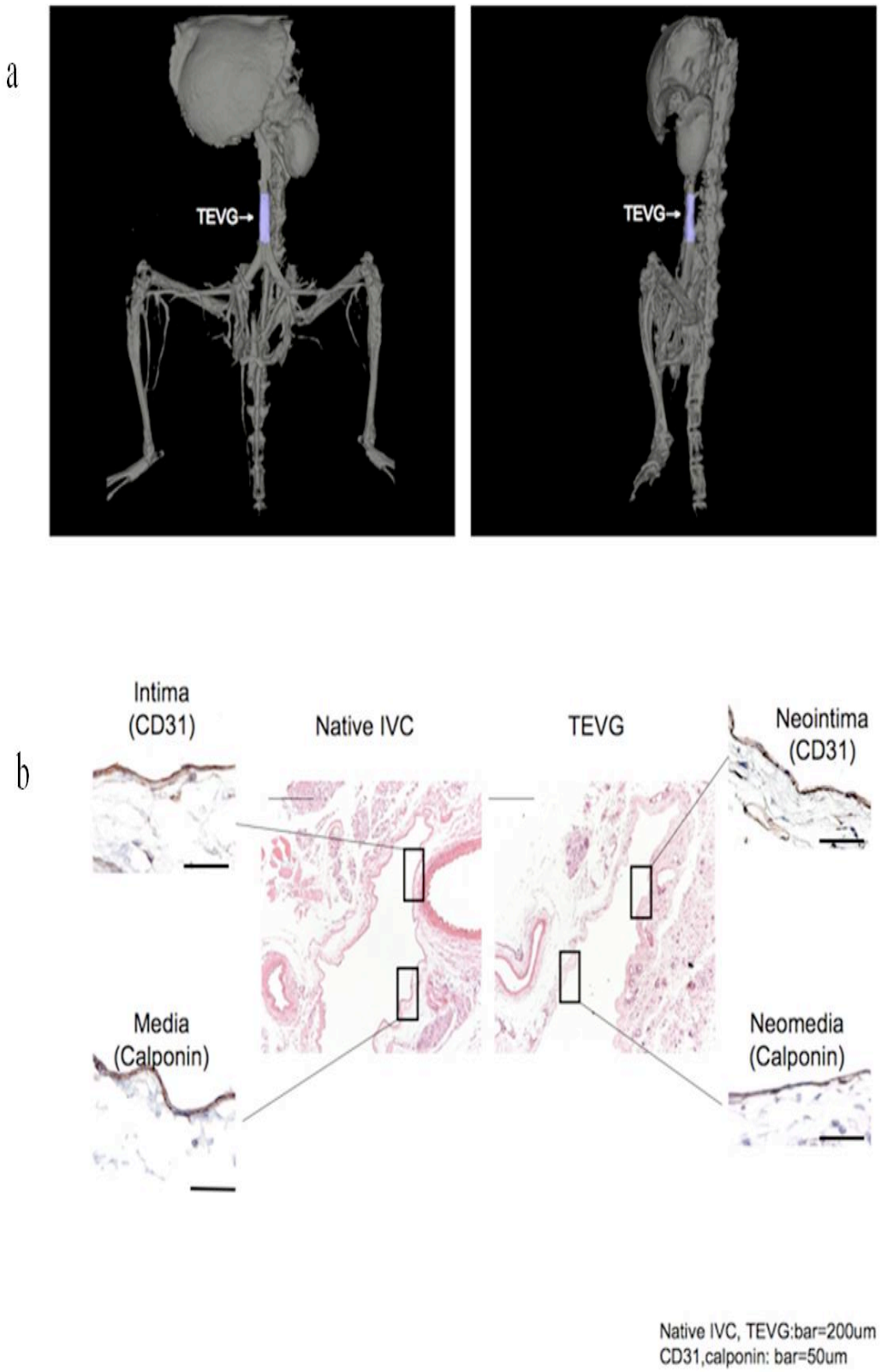
a
TEVG
TEVG
b
Intima
(CD31)
Native IVC
TEVG
Neointima
(CD31)
Media
(Calponin)
Neomedia
(Calponin)
Native IVC, TEVG:bar=200um
CD31,calponin: bar=50um

Figure 7

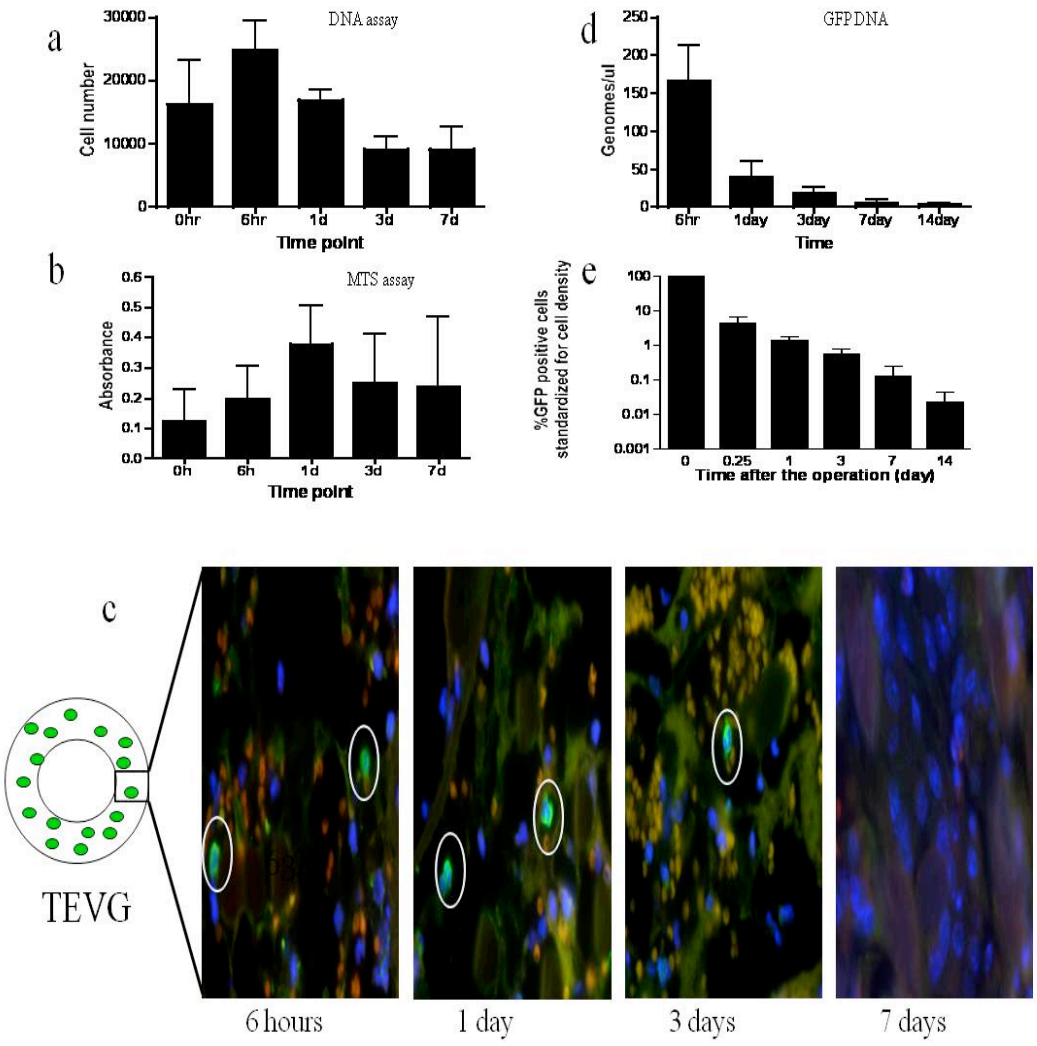
a
DNA assay
Cell number
30000
20000
10000
0
0hr
6hr
1d
3d
7d
Time point
d
GFP DNA
Genomes/ul
250
200
150
100
50
0
6hr
1day
3day
7day
14day
Time
b
MTS assay
Absorbance
0.6
0.5
0.4
0.3
0.2
0.1
0.0
0h
6h
1d
3d
7d
Time point
e
%GFP positive cells standardized for cell density
100
10
1
0.1
0.01
0.001
0
0.25
1
3
7
14
Time after the operation (day)
c
TEVG
6 hours
1 day
3 days
7 days

Figure 8

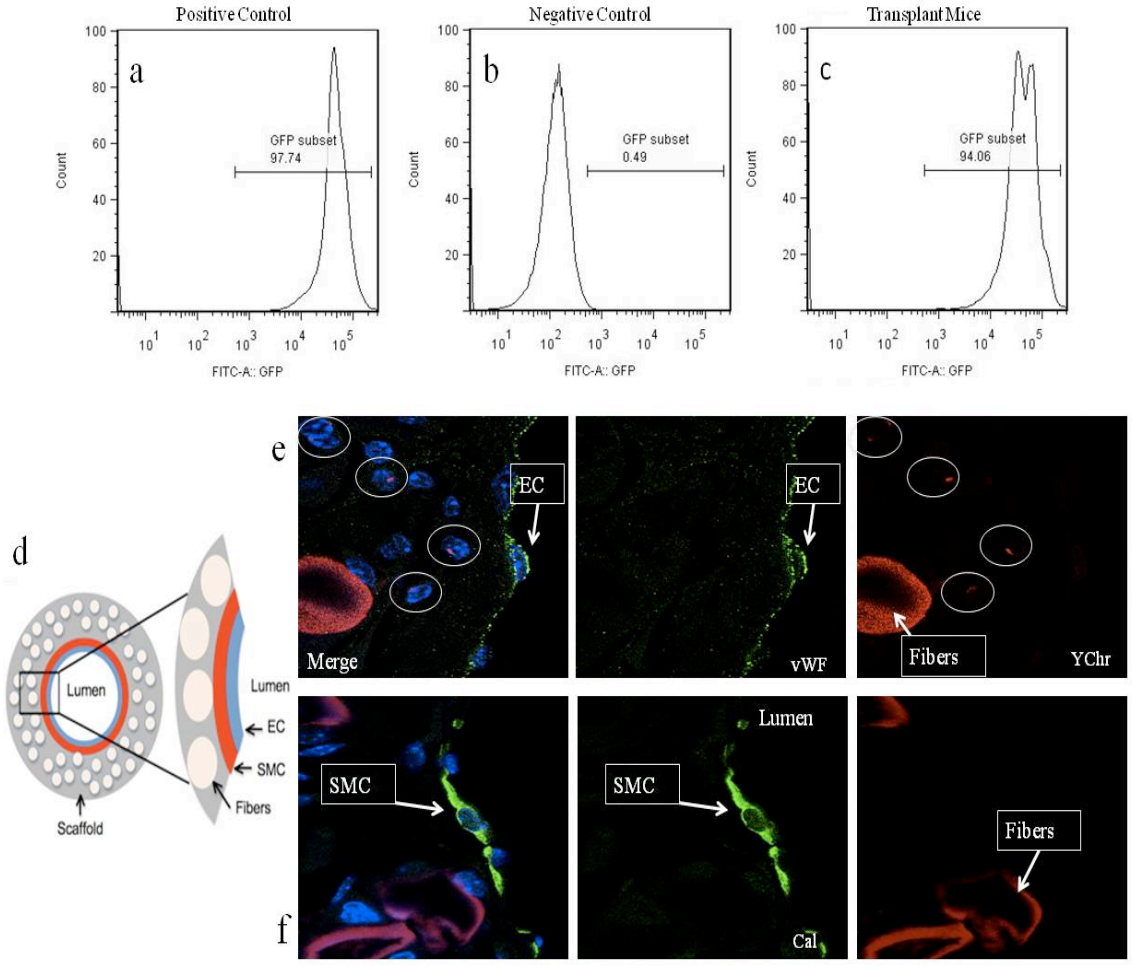
Positive Control
Negative Control
Transplant Mice
a
b
c
GFP subset
97.74
GFP subset
0.49
GFP subset
94.06
Count
FITC-A:: GFP
d
Lumen
Scaffold
Lumen
EC
SMC
Fibers
e
EC
Merge
vWF
Fibers
YChr
f
SMC
Lumen
Cal

Figure 9

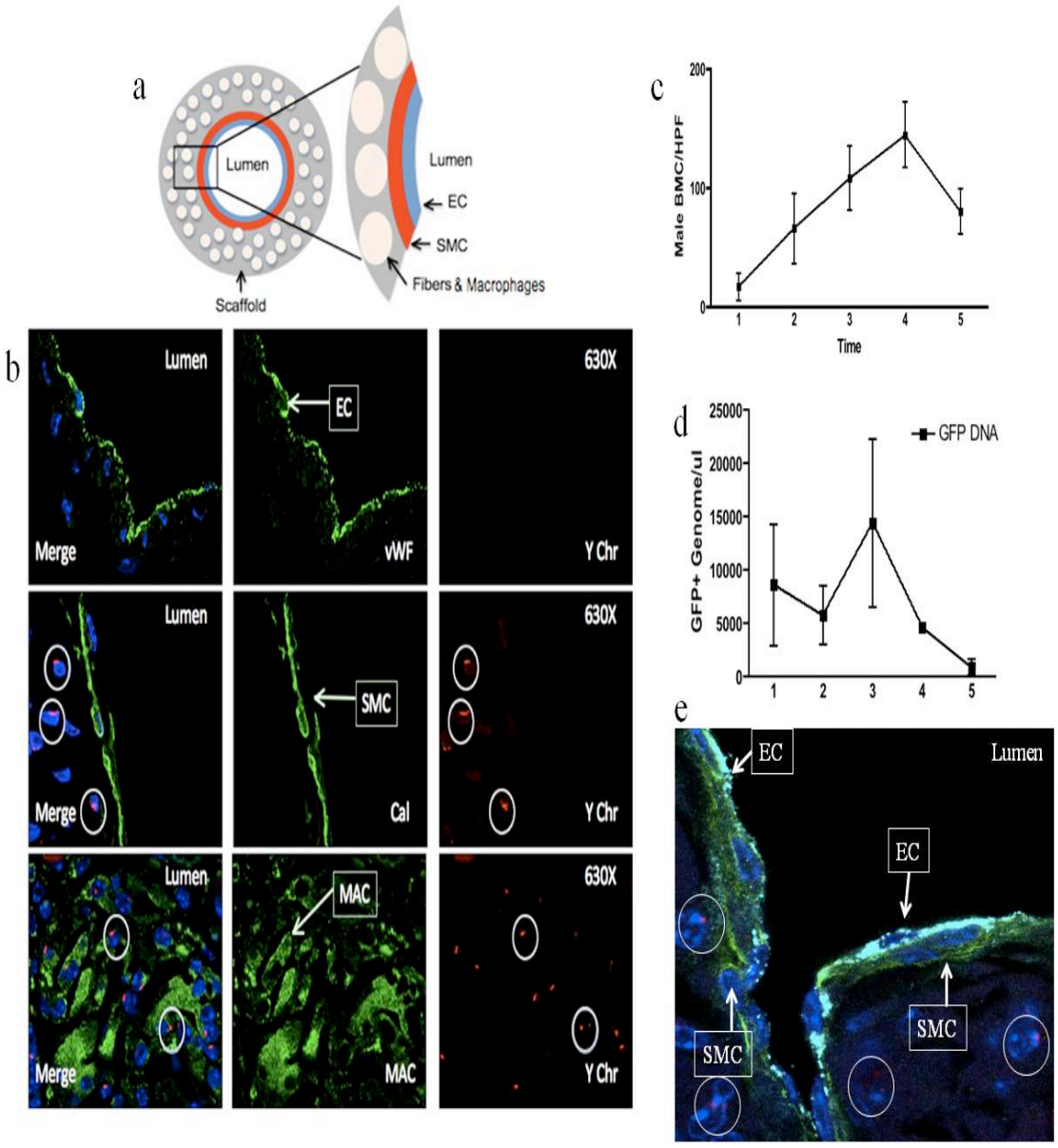
a
Lumen
Lumen
EC
SMC
Fibers & Macrophages
Scaffold
b
Lumen
EC
630X
Merge
vWF
Y Chr
Lumen
SMC
630X
Merge
Cal
Y Chr
Lumen
MAC
630X
Merge
MAC
Y Chr
c
Male BMC/HPF
200
100
0
1
2
3
4
5
Time
d
GFP DNA
GFP+ Genome/ul
25000
20000
15000
10000
5000
0
1
2
3
4
5
e
EC
Lumen
EC
SMC
SMC

Figure 10

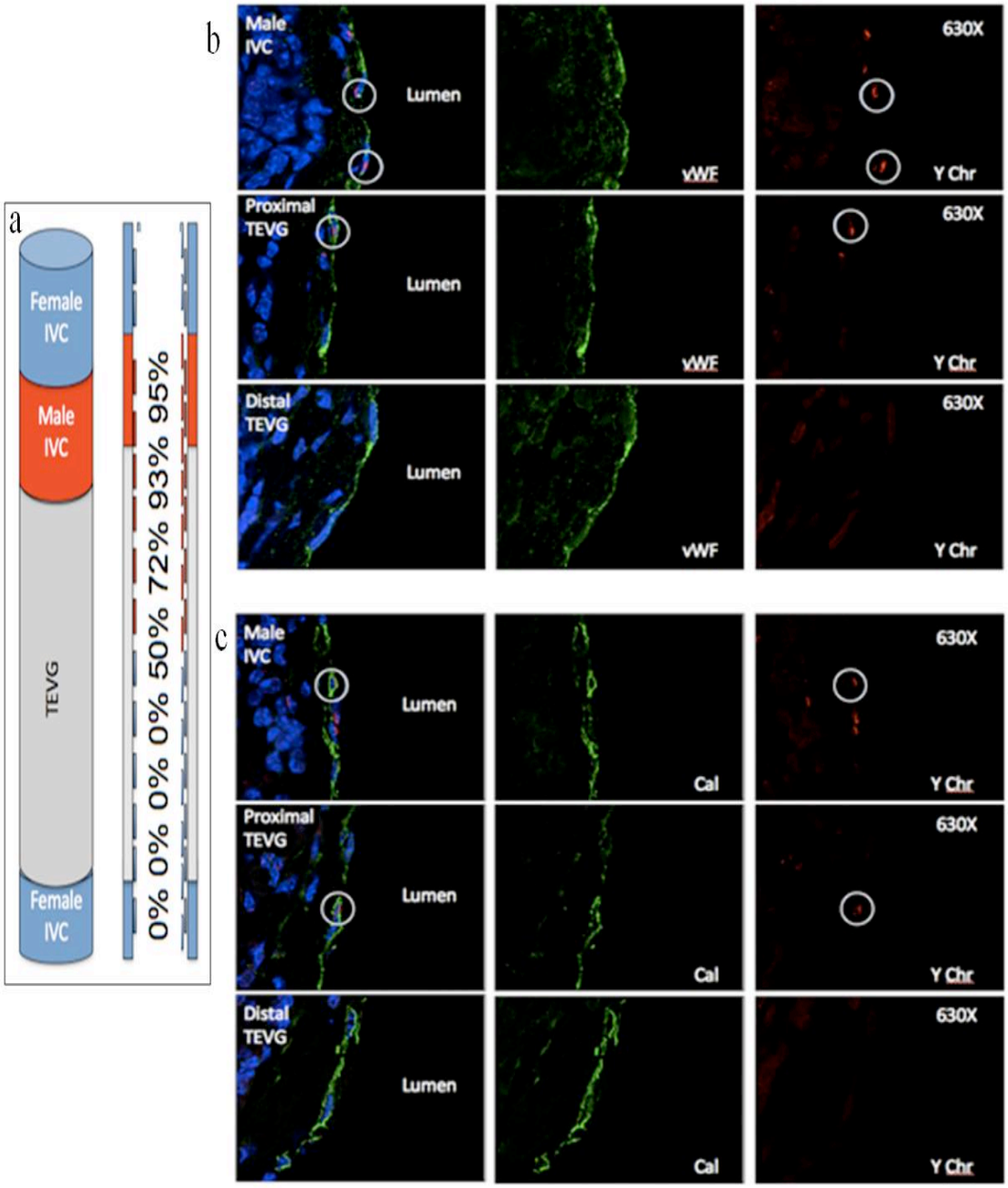
a
Female IVC
Male IVC
TEVG
Female IVC
0% 0% 0% 0% 50% 72% 93% 95%
b
Male IVC
Lumen
vWF
630X
Y Chr
Proximal TEVG
Lumen
vWF
630X
Y Chr
Distal TEVG
Lumen
vWF
630X
Y Chr
c
Male IVC
Lumen
Cal
630X
Y Chr
Proximal TEVG
Lumen
Cal
630X
Y Chr
Distal TEVG
Lumen
Cal
630X
Y Chr

Figure Legends

Figure 1: Human TEVG, constructed from hBMC-seeded scaffolds, transform into living blood vessels in the SCID/bg mouse. **A)** Micro-CT angiography at wk 10 shows a patent TEVG functioning as an IVC venous conduit. Gross images of a human TEVG interposed into the SCID/bg mouse IVC at **B)** operative day 0 and **C)** after 24 wks *in vivo*. **D)** Gross image of native mouse IVC for comparison. Corresponding H&E images of **E)** TEVG at day 0 (demonstrating hBMC transplanted into scaffold wall), **F)** TEVG at 24 wks (notice scaffold material has degraded), and **G)** native mouse IVC. Low magnification (100X) photomicrographs of TEVG at 10wks post-implantation show scaffold material still present, and the development of a confluent **H)** smooth muscle cell (αSMA=brown) layer and **I)** endothelial cell (vWF=brown) lining throughout the inner lumen. By 24wks, scaffold material has degraded and TEVG displays mature vessel architecture. **J)** High magnification (400X) photomicrograph demonstrates an organized endothelial intima (vWF=red) and SMC media (αSMA=green). **K)** Low magnification (100X) photomicrograph of Verhoeff van Gieson stain shows scaffold has been replaced by a circumferentially oriented supportive adventitial layer composed of collagen (collagen=pink). **L)** High magnification (400X) Verhoeff van Gieson stain demonstrates organization of collagen fibrils, but no elastin fibers (elastin=black, collagen=pink).

Figure 2: Seeded hBMC do not directly contribute to the cellularity of the developing neovessel. Immunohistochemical analysis of pre-implant TEVG shows evidence of **A)** human leukocytes (hCD45), **B)** human EC (hCD31), and **C)** human stem cells (hCD34). Immunohistochemical analysis of hBMC-seeded scaffolds explanted at 1wk *in vivo* detected only small numbers of retained **D)** human monocytes (hCD68) and **E)** human EC (hCD31). No hCD34 was detectable. After 1 wk, no human antigen expression in the TEVG was detectable via immunohistochemistry. **F)** Majority of cells in scaffold wall at 1 wk express F4/80, a marker for mouse monocytes/macrophages. **G)** Smooth muscle actin (αSMA) expression starts to be detected around the inner luminal lining by 1wk. **H)** Patchy endothelialization, indicated by positive vWF expression, begins to form in the inner lumen by 3 wks. **I)** RT-PCR of explanted hBMC-seeded scaffolds confirms no detectable human RNA expression after 1 wk *in vivo*. All photomicrographs at 400X magnification (brown = positive expression). Data in graphs expressed as mean ± SD, * $p<0.05$ ** $p<0.001$.

Figure 3: Seeded hBMC increase early monocyte recruitment and secrete MCP-1. **A)** Although seeded hBMC are no longer present after 1 wk *in vivo*, scaffold cellularity rapidly increases during the first week of development, and then stabilizes until scaffold degradation. Comparison between hBMC-seeded and unseeded scaffolds shows that hBMC seeding increases early cellularity at 1 wk. **B)** The difference in cellularity between hBMC-seeded and unseeded scaffolds at wk 1 is primarily due to significantly increased numbers of mouse monocytes (positive F4/80 expression). **C-E)** Scaffold exposure activates hBMC to produce multiple cytokines associated with monocyte chemotaxis. Luminex assay shows increased expression levels of 12 of the 17 cytokines evaluated when hBMC are seeded onto PGA-P(CL/LA) scaffolds. MCP-1 was expressed in the highest concentration, with log fold differences over the other cytokines tested. IP-

10 and PDGF expression are notably decreased by exposure to PGA-P(CL/LA) scaffolds. **F)** Confirmatory MCP-1 specific ELISA shows significant increase in MCP-1 production when hBMC seeded onto PGA-P(CL/LA) scaffolds. Data in graphs expressed as mean ± SD, * $p<0.05$, ** $p<0.001$.

Figure 4: MCP-1 releasing microparticles mimic function of seeded hBMC by increasing early monocyte recruitment. To investigate the potential role of MCP-1 secreted by seeded hBMC, MCP-1-releasing microparticles were constructed from biodegradable alginate. Scanning electron microscopy images of **A)** MCP-1 microparticles similar in size distribution to hBMC (1-20μm), **B)** scaffold embedded with MCP-1 microparticles, and **C)** higher magnification of scaffold, demonstrating individual PGA fibers with MCP-1 microparticles securely embedded into the P(CL/LA) sealant. **D)** Cumulative MCP-1 release profile of MCP-1 microparticle scaffolds (n=5) shows they release approximately 200ng MCP-1 over 72hrs. **E)** At 1wk, MCP-1 microparticle scaffolds (n=3) have significantly greater numbers of mouse monocytes (F4/80 positive cells) than both hBMC-seeded (n=5) and unseeded scaffolds (n=5). At 10wks, all MCP-1 microparticle scaffolds (n=5) were patent and demonstrated similar vascular architecture to hBMC-seeded scaffolds. **F)** Immunohistochemical staining of the vWF antigen shows a confluent endothelial intimal layer. **G)** An organizing smooth muscle media layer, identified by α-SMA expression, was detectable below the intima. **H)** Gamori trichrome staining shows supportive circumferentially oriented collagen fibrils within the vascular neotissue and an external ring of degrading scaffold material. Photomicrographs of hBMC-seeded scaffold stained with **I)** vWF, **J)** α-SMA, and **K)** Gamori trichrome, for comparison. All histologic photomicrographs at 400X magnification. Data in graphs expressed as mean ± SD; *$p<0.05$, **$p<0.001$.

Figure 5: Proposed mechanism of vascular transformation of TEVG composed from hBMC-seeded biodegradable scaffolds. **A)** An early pulse of MCP-1, secreted from seeded hBMC, enhances early monocyte recruitment to the scaffold. Activated monocytes then release multiple angiogenic cytokines and growth factors, i.e. VEGF, which recruits SMC and EC to the scaffold. Vascular cells potentially come from circulating progenitors and/or proliferation/migration of mature vascular cells in the adjacent vessel segments. EC and SMC appropriately organize into a mature blood vessel structure on the luminal surface of the scaffold. As the scaffold degrades, monocytes migrate away, leaving behind a completely autologous neovessel. **B)** Immunohistochemical VEGF staining of hBMC-seeded scaffolds at post-implantation wks 1, 6, and 10 shows continued VEGF expression throughout TEVG development (brown = positive VEGF expression). All photomicrographs at 400X magnification.

Table 1: Flow cytometry characterization of human bone marrow mononuclear cells used for seeding biodegradable scaffolds. Data accumulated from five different donors and expressed as mean ± SD.

Figure 6: Representative CT angiogram of a TEVG IVC interposition graft six-months after implantation (a). TEVG colored blue. Representative photomicrographs of

immunohistochemical characterization of the native IVC compared to the TEVG six-months after implantation (H&E 100X) and (CD31 & Cal 400X) (b).

Figure 7: DNA Assay of scaffolds from 0 hr to 7 days of in vitro incubation, showed increased number of cells in first 24 hours and loss of cells after 72 hours (a). MTS Assay of scaffolds from 0 hr to 7 days in vitro incubation, showed initial increase in metabolic activity followed by steady state (b). Invivo tracking using immunofluorescence (630X) demonstrated GFP positive cells within the graft at 6 hours, 1 and 3 days, but no cells 7 days post-implantation (c). These findings were corroborated by qPCR of GFP DNA from TEVG (N=30) seeded with GFP positive cells, implanted in GFP negative hosts, and harvested between 6 hours and 14 days after implantation (d). Level of detection is 10 genomes/ul. Data in the graph are expressed as mean ± standard deviation. Percentage of GFP-labeled cells per TEVG standardized for cell density decrease from 4.37% at 6-hours to 0.02% at 14-days (e).

Figure 8: FACS analysis of GFP (+) mouse as positive control (a), C57BL/6 mouse for negative control (b) and engraftment 5-weeks post-transplantation (c). Schematic demonstrating components and orientation of photomicrographs for e and f (d).Confocal microscopic images of TEVG implanted into female host that had undergone transplantation with male bone marrow harvested 14-days after implantation demonstrating no co-localization with the Y chromosome (Y-chromosome FISH) and either (EC) endothelial cells (von Willebrand Factor, vWF, 630X) (e) or (SMC) smooth muscle cells (Calponin 630X)(f).

Figure 9: Schematic demonstrating components and orientation of photomicrographs for b (a). Confocal microscopic images of TEVG implanted into female host that had undergone transplantation with male bone marrow harvested six-months after implantation demonstrating co-localization of macrophages (MAC) and the Y-chromosome (Y-chromosome FISH) but no co-localization with the Y chromosome (Y-chromosome FISH) and either endothelial cells (von Willebrand Factor) or smooth muscle cells (Calponin) (400X) (b). The numbers of infiltrating BM-derived Y

chromosome (Y-chromosome FISH) cells (Bone marrow cells/High power field)in the graft wall increased up to 10 weeks, while graft degradation is occurring, but at 6 months post-implantation these cells markedly decrease (c). This was quantified and corroborated using qPCR for GFP DNA within the graft over a six-month period (d). Confocal microscopic image of triple staining of a six-month neovessel with normal IVC configuration with single layer neointima (EC: vWF/light blue), neomedia (SMC: calponin/green) and neoadventiacia with scattered inflamatory cells (Male: Ychr/red) (e).

Figure 10: Schematic demonstrating composite TEVG (N=8) created by anastomosing a syngeneic male IVC with a TEVG and implanted into a female host harvested six-months after implantation and the percentage of cells with Y-chromosome as a function of distance from the male IVC (a). Confocal microscopic images of demonstrating co-localization of endothelial cells (von Willebrand Factor) and Y Chromosome (Y-chromosome FISH)(400X) (b). Photomicrographs demonstrating co-localization of smooth muscle cells (calponin) and Y Chromosome (Y-chromosome FISH) (400X) (c).

Part VI. References

1. Saposnik, G., Goodman, S. G., Leiter, L. A., et al. Applying the evidence: do patients with stroke, coronary artery disease, or both achieve similar treatment goals? *Stroke* 40: 1417-1424, 2009.

2. Association, A. H. Cardiovascular Disease Cost. 2009.

3. Organization, W. H. Global Burden of Disease. 2004.

4. Desai, N. D., Fremes, S. E. Radial artery conduit for coronary revascularization: as good as an internal thoracic artery? *Curr Opin Cardiol* 22: 534-540, 2007.

5. Malvindi, P. G., Jacob, S., Kallikourdis, A., et al. What is the patency of the gastroepiploic artery when used for coronary artery bypass grafting? *Interact Cardiovasc Thorac Surg* 6: 397-402, 2007.

6. Dashwood, M. R., Loesch, A. The saphenous vein as a bypass conduit: the potential role of vascular nerves in graft performance. *Curr Vasc Pharmacol* 7: 47-57, 2009.

7. Hong, Y. J., Mintz, G. S., Kim, S. W., et al. Disease progression in nonintervened saphenous vein graft segments a serial intravascular ultrasound analysis. *J Am Coll Cardiol* 53: 1257-1264, 2009.

8. Carrel, A., Lindbergh, C. A. The Culture of Whole Organs. *Science* 81: 621-623, 1935.

9. Weinberg, C. B., Bell, E. A blood vessel model constructed from collagen and cultured vascular cells. *Science* 231: 397-400, 1986.

10. Voorhees, A. B., Jr., Jaretzki, A., 3rd, Blakemore, A. H. The use of tubes constructed from vinyon "N" cloth in bridging arterial defects. *Ann Surg* 135: 332-336, 1952.

11. Blakemore, A. H., Voorhees, A. B., Jr. The use of tubes constructed from vinyon N cloth in bridging arterial defects; experimental and clinical. *Ann Surg* 140: 324-334, 1954.

12. Lanza, R. P., Langer, R. S., Vacanti, J. *Principles of tissue engineering*, 3rd Ed. Burlington, MA: Elsevier Academic Press, 2007.

13. Callow, A. D. Arterial homografts. *Eur J Vasc Endovasc Surg* 12: 272-281, 1996.

14. Shinoka, T., Shum-Tim, D., Ma, P. X., et al. Creation of viable pulmonary artery autografts through tissue engineering. *J Thorac Cardiovasc Surg* 115: 536-545; discussion 545-536, 1998.

15. L'Heureux, N., Paquet, S., Labbe, R., et al. A completely biological tissue-engineered human blood vessel. *FASEB J* 12: 47-56, 1998.

16. Niklason, L. E., Gao, J., Abbott, W. M., et al. Functional arteries grown in vitro. *Science* 284: 489-493, 1999.

17. Shum-Tim, D., Stock, U., Hrkach, J., et al. Tissue engineering of autologous aorta using a new biodegradable polymer. *Ann Thorac Surg* 68: 2298-2304; discussion 2305, 1999.

18. Shin'oka, T., Imai, Y., Ikada, Y. Transplantation of a tissue-engineered pulmonary artery. *N Engl J Med* 344: 532-533, 2001.

19. L'Heureux, N., McAllister, T. N., de la Fuente, L. M. Tissue-engineered blood vessel for adult arterial revascularization. *N Engl J Med* 357: 1451-1453, 2007.

20. L'Heureux, N., Dusserre, N., Marini, A., et al. Technology insight: the evolution of tissue-engineered vascular grafts--from research to clinical practice. *Nat Clin Pract Cardiovasc Med* 4: 389-395, 2007.

21. Sarkar, S., Schmitz-Rixen, T., Hamilton, G., et al. Achieving the ideal properties for vascular bypass grafts using a tissue engineered approach: a review. *Med Biol Eng Comput* 45: 327-336, 2007.

22. Brennan, M. P., Dardik, A., Hibino, N., et al. Tissue-engineered vascular grafts demonstrate evidence of growth and development when implanted in a juvenile animal model. *Ann Surg* 248: 370-377, 2008.

23. Gildein, H. P., Ahmadi, A., Fontan, F., et al. Special problems in Fontan-type operations for complex cardiac lesions. *Int J Cardiol* 29: 21-28, 1990.

24. Shinoka, T., Breuer, C. K., Tanel, R. E., et al. Tissue engineering heart valves: valve leaflet replacement study in a lamb model. *Ann Thorac Surg* 60: S513-516, 1995.

25. Shinoka, T., Shum-Tim, D., Ma, P. X., et al. Tissue-engineered heart valve leaflets: does cell origin affect outcome? *Circulation* 96: II-102-107, 1997.

26. Breuer, C. K., Shin'oka, T., Tanel, R. E., et al. Tissue engineering lamb heart valve leaflets. *Biotechnol Bioeng* 50: 562-567, 1996.

27. Zund, G., Breuer, C. K., Shinoka, T., et al. The in vitro construction of a tissue engineered bioprosthetic heart valve. *Eur J Cardiothorac Surg* 11: 493-497, 1997.

28. Shinoka, T., Ma, P. X., Shum-Tim, D., et al. Tissue-engineered heart valves. Autologous valve leaflet replacement study in a lamb model. *Circulation* 94: II164-168, 1996.

29. Breuer, C. K., Mettler, B. A., Anthony, T., et al. Application of tissue-engineering principles toward the development of a semilunar heart valve substitute. *Tissue Eng* 10: 1725-1736, 2004.

30. Nerem, R. M. Tissue engineering a blood vessel substitute: the role of biomechanics. *Yonsei Med J* 41: 735-739, 2000.

31. Riha, G. M., Lin, P. H., Lumsden, A. B., et al. Review: application of stem cells for vascular tissue engineering. *Tissue Eng* 11: 1535-1552, 2005.

32. Matsumura, G., Miyagawa-Tomita, S., Shin'oka, T., et al. First evidence that bone marrow cells contribute to the construction of tissue-engineered vascular autografts in vivo. *Circulation* 108: 1729-1734, 2003.

33. Watanabe, M., Shin'oka, T., Tohyama, S., et al. Tissue-engineered vascular autograft: inferior vena cava replacement in a dog model. *Tissue Eng* 7: 429-439, 2001.

34. Naito, Y., Imai, Y., Shin'oka, T., et al. Successful clinical application of tissue-engineered graft for extracardiac Fontan operation. *J Thorac Cardiovasc Surg* 125: 419-420, 2003.

35. Shin'oka, T., Matsumura, G., Hibino, N., et al. Midterm clinical result of tissue-engineered vascular autografts seeded with autologous bone marrow cells. *J Thorac Cardiovasc Surg* 129: 1330-1338, 2005.

36. L'Heureux, N., Germain, L., Labbe, R., et al. In vitro construction of a human blood vessel from cultured vascular cells: a morphologic study. *J Vasc Surg* 17: 499-509, 1993.

37. L'Heureux, N., Stoclet, J. C., Auger, F. A., et al. A human tissue-engineered vascular media: a new model for pharmacological studies of contractile responses. *FASEB J* 15: 515-524, 2001.

38. L'Heureux, N., Dusserre, N., Konig, G., et al. Human tissue-engineered blood vessels for adult arterial revascularization. *Nat Med* 12: 361-365, 2006.

39. McAllister, T. N., Maruszewski, M., Garrido, S. A., et al. Effectiveness of haemodialysis access with an autologous tissue-engineered vascular graft: a multicentre cohort study. *Lancet* 373: 1440-1446, 2009.

40. Hanjaya-Putra, D., Gerecht, S. Vascular engineering using human embryonic stem cells. *Biotechnol Prog* 25: 2-9, 2009.

41. Cuenca-Lopez, M. D., Zamora-Navas, P., Garcia-Herrera, J. M., et al. Adult stem cells applied to tissue engineering and regenerative medicine. *Cell Mol Biol (Noisy-le-grand)* 54: 40-51, 2008.

42. Yamahara, K., Itoh, H. Potential use of endothelial progenitor cells for regeneration of the vasculature. *Ther Adv Cardiovasc Dis* 3: 17-27, 2009.

43. Nourse, M. B., Halpin, D. E., Scatena, M., et al. VEGF induces differentiation of functional endothelium from human embryonic stem cells: implications for tissue engineering. *Arterioscler Thromb Vasc Biol* 30: 80-89.

44. Harris, L. J., Abdollahi, H., Zhang, P., et al. Differentiation of Adult Stem Cells into Smooth Muscle for Vascular Tissue Engineering. *J Surg Res*, 2009.

45. Noghero, A., Bussolino, F., Gualandris, A. Role of the microenvironment in the specification of endothelial progenitors derived from embryonic stem cells. *Microvasc Res*.

46. Xiao, Q., Luo, Z., Pepe, A. E., et al. Embryonic stem cell differentiation into smooth muscle cells is mediated by Nox4-produced H2O2. *Am J Physiol Cell Physiol* 296: C711-723, 2009.

47. Matsumura, G., Hibino, N., Ikada, Y., et al. Successful application of tissue engineered vascular autografts: clinical experience. *Biomaterials* 24: 2303-2308, 2003.

48. Noishiki, Y., Tomizawa, Y., Yamane, Y., et al. Autocrine angiogenic vascular prosthesis with bone marrow transplantation. *Nat Med* 2: 90-93, 1996.

49. McKay, R. Stem cells--hype and hope. *Nature* 406: 361-364, 2000.

50. Shintani, S., Murohara, T., Ikeda, H., et al. Mobilization of endothelial progenitor cells in patients with acute myocardial infarction. *Circulation* 103: 2776-2779, 2001.

51. Hibino, N., McGillicuddy, E., Matsumura, G., et al. Late-term results of tissue-engineered vascular grafts in humans. *J Thorac Cardiovasc Surg* 139: 431-436, 436 e431-432.

52. Roh, J. Gylcolmethacrylate is superior to methylmethacrylate for h2istologic evaluation of biodegradable polymer scaffolds used for vascular tissue engineering. *J Histotechnology* 29: 245-252, 2006.

53. Tuchschmidt, J., Mecher, C., Wagers, P., et al. Elevated pulmonary capillary wedge pressure in a patient with hypovolemia. *J Clin Monit* 3: 67-69, 1987.

54. Ziegelhoeffer, T., Fernandez, B., Kostin, S., et al. Bone marrow-derived cells do not incorporate into the adult growing vasculature. *Circ Res* 94: 230-238, 2004.

55. Zentilin, L., Tafuro, S., Zacchigna, S., et al. Bone marrow mononuclear cells are recruited to the sites of VEGF-induced neovascularization but are not incorporated into the newly formed vessels. *Blood* 107: 3546-3554, 2006.

56. Murry, C. E., Soonpaa, M. H., Reinecke, H., et al. Haematopoietic stem cells do not transdifferentiate into cardiac myocytes in myocardial infarcts. *Nature* 428: 664-668, 2004.

57. Balsam, L. B., Wagers, A. J., Christensen, J. L., et al. Haematopoietic stem cells adopt mature haematopoietic fates in ischaemic myocardium. *Nature* 428: 668-673, 2004.

58. Wagers, A. J., Sherwood, R. I., Christensen, J. L., et al. Little evidence for developmental plasticity of adult hematopoietic stem cells. *Science* 297: 2256-2259, 2002.

59. Kinnaird, T., Stabile, E., Burnett, M. S., et al. Local delivery of marrow-derived stromal cells augments collateral perfusion through paracrine mechanisms. *Circulation* 109: 1543-1549, 2004.

60. Uemura, R., Xu, M., Ahmad, N., et al. Bone marrow stem cells prevent left ventricular remodeling of ischemic heart through paracrine signaling. *Circ Res* 98: 1414-1421, 2006.

61. Gnecchi, M., He, H., Liang, O. D., et al. Paracrine action accounts for marked protection of ischemic heart by Akt-modified mesenchymal stem cells. *Nat Med* 11: 367-368, 2005.

62. O'Neill, T. J. t., Wamhoff, B. R., Owens, G. K., et al. Mobilization of bone marrow-derived cells enhances the angiogenic response to hypoxia without transdifferentiation into endothelial cells. *Circ Res* 97: 1027-1035, 2005.

63. Kinnaird, T., Stabile, E., Burnett, M. S., et al. Marrow-derived stromal cells express genes encoding a broad spectrum of arteriogenic cytokines and promote in vitro and in vivo arteriogenesis through paracrine mechanisms. *Circ Res* 94: 678-685, 2004.

64. Terada, N., Hamazaki, T., Oka, M., et al. Bone marrow cells adopt the phenotype of other cells by spontaneous cell fusion. *Nature* 416: 542-545, 2002.

65. Ying, Q. L., Nichols, J., Evans, E. P., et al. Changing potency by spontaneous fusion. *Nature* 416: 545-548, 2002.

66. Alvarez-Dolado, M., Pardal, R., Garcia-Verdugo, J. M., et al. Fusion of bone-marrow-derived cells with Purkinje neurons, cardiomyocytes and hepatocytes. *Nature* 425: 968-973, 2003.

67. Nygren, J. M., Jovinge, S., Breitbach, M., et al. Bone marrow-derived hematopoietic cells generate cardiomyocytes at a low frequency through cell fusion, but not transdifferentiation. *Nat Med* 10: 494-501, 2004.

68. Hibino, N., Shin'oka, T., Matsumura, G., et al. The tissue-engineered vascular graft using bone marrow without culture. *J Thorac Cardiovasc Surg* 129: 1064-1070, 2005.

69. Brennan, M. P., Dardik, A., Hibino, N., et al. Tissue-engineered Vascular Grafts Demonstrate Evidence of Growth and Development When Implanted in a Juvenile Animal Model. *Transactions of the ... Meeting of the American Surgical Association* 126: 20-27, 2008.

70. Matsumura, G., Ishihara, Y., Miyagawa-Tomita, S., et al. Evaluation of tissue-engineered vascular autografts. *Tissue Eng* 12: 3075-3083, 2006.

71. Isomatsu, Y., Shin'oka, T., Matsumura, G., et al. Extracardiac total cavopulmonary connection using a tissue-engineered graft. *J Thorac Cardiovasc Surg* 126: 1958-1962, 2003.

72. Arras, M., Ito, W. D., Scholz, D., et al. Monocyte activation in angiogenesis and collateral growth in the rabbit hindlimb. *J Clin Invest* 101: 40-50, 1998.

73. Heil, M., Ziegelhoeffer, T., Pipp, F., et al. Blood monocyte concentration is critical for enhancement of collateral artery growth. *Am J Physiol Heart Circ Physiol* 283: H2411-2419, 2002.

74. Bergmann, C. E., Hoefer, I. E., Meder, B., et al. Arteriogenesis depends on circulating monocytes and macrophage accumulation and is severely depressed in op/op mice. *J Leukoc Biol* 80: 59-65, 2006.

75. Scholz, D., Ito, W., Fleming, I., et al. Ultrastructure and molecular histology of rabbit hind-limb collateral artery growth (arteriogenesis). *Virchows Arch* 436: 257-270, 2000.

76. Heil, M., Ziegelhoeffer, T., Wagner, S., et al. Collateral artery growth (arteriogenesis) after experimental arterial occlusion is impaired in mice lacking CC-chemokine receptor-2. *Circ Res* 94: 671-677, 2004.

77. Voskuil, M., van Royen, N., Hoefer, I. E., et al. Modulation of collateral artery growth in a porcine hindlimb ligation model using MCP-1. *Am J Physiol Heart Circ Physiol* 284: H1422-1428, 2003.

78. van Royen, N., Hoefer, I., Bottinger, M., et al. Local monocyte chemoattractant protein-1 therapy increases collateral artery formation in apolipoprotein E-deficient mice but induces systemic monocytic CD11b expression, neointimal formation, and plaque progression. *Circ Res* 92: 218-225, 2003.

79. Ito, W. D., Arras, M., Winkler, B., et al. Monocyte chemotactic protein-1 increases collateral and peripheral conductance after femoral artery occlusion. *Circ Res* 80: 829-837, 1997.

80. Moldovan, N. I., Goldschmidt-Clermont, P. J., Parker-Thornburg, J., et al. Contribution of monocytes/macrophages to compensatory neovascularization: the drilling of metalloelastase-positive tunnels in ischemic myocardium. *Circ Res* 87: 378-384, 2000.

81. Rehman, J., Li, J., Orschell, C. M., et al. Peripheral blood "endothelial progenitor cells" are derived from monocyte/macrophages and secrete angiogenic growth factors. *Circulation* 107: 1164-1169, 2003.

82. Grunewald, M., Avraham, I., Dor, Y., et al. VEGF-induced adult neovascularization: recruitment, retention, and role of accessory cells. *Cell* 124: 175-189, 2006.

83. Alon, T., Hemo, I., Itin, A., et al. Vascular endothelial growth factor acts as a survival factor for newly formed retinal vessels and has implications for retinopathy of prematurity. *Nat Med* 1: 1024-1028, 1995.

84. Asahara, T., Masuda, H., Takahashi, T., et al. Bone marrow origin of endothelial progenitor cells responsible for postnatal vasculogenesis in physiological and pathological neovascularization. *Circ Res* 85: 221-228, 1999.

85. Zouggari, Y., Ait-Oufella, H., Waeckel, L., et al. Regulatory T cells modulate postischemic neovascularization. *Circulation* 120: 1415-1425, 2009.

86. van Weel, V., Toes, R. E., Seghers, L., et al. Natural killer cells and CD4+ T-cells modulate collateral artery development. *Arterioscler Thromb Vasc Biol* 27: 2310-2318, 2007.

87. Roh, J. D., Sawh-Martinez, R., Brennan, M. P., et al. Tissue-engineered vascular grafts transform into mature blood vessels via an inflammation-mediated process of vascular remodeling. *Proc Natl Acad Sci U S A* 107: 4669-4674.